RADC-TR-88-279
Final Technical Report
December 1988

RADIATION HARDENED SILICA-BASED OPTICAL FIBERS

GTE Laboratories

W.J. Miniscalco, T. Wei, and P.K. Onorato

ROME AIR DEVELOPMENT CENTER
Air Force Systems Command
Griffiss Air Force Base, NY 13441-5700

This report has been reviewed by the RADC Public Affairs Division (PA) and is releasable to the National Technical Information Service (NTIS). At NTIS it will be releasable to the general public, including foreign nations.

RADC-TR-88-279 has been reviewed and is approved for publication.

APPROVED: //

JAMES A. WALL
Project Engineer

APPROVED: Harold Roth

HAROLD ROTH
Director of Solid State Sciences

FOR THE COMMANDER: James W. Hyde III

JAMES W. HYDE III
Directorate of Plans & Programs

If your address has changed or if you wish to be removed from the RADC mailing list, or if the addressee is no longer employed by your organization, please notify RADC (ESR) Hanscom AFB MA 01731-5000. This will assist us in maintaining a current mailing list.

Do not return copies of this report unless contractual obligations or notices on a specific document require that it be returned.

UNCLASSIFIED

SECURITY CLASSIFICATION OF THIS PAGE

REPORT DOCUMENTATION PAGE

Form Approved OMB No. 0704-0188

1a. REPORT SECURITY CLASSIFICATION UNCLASSIFIED	1b. RESTRICTIVE MARKINGS N/A
2a. SECURITY CLASSIFICATION AUTHORITY N/A	3. DISTRIBUTION/AVAILABILITY OF REPORT Approved for public release; distribution unlimited.
2b. DECLASSIFICATION/DOWNGRADING SCHEDULE N/A	
4. PERFORMING ORGANIZATION REPORT NUMBER(S) N/A	5. MONITORING ORGANIZATION REPORT NUMBER(S) RADC-TR-88-279
6a. NAME OF PERFORMING ORGANIZATION GTE Laboratories Incorporated 6b. OFFICE SYMBOL (If applicable)	7a. NAME OF MONITORING ORGANIZATION Rome Air Development Center (ESR)
6c. ADDRESS (City, State, and ZIP Code) 40 Sylvan Road Waltham MA 02254	7b. ADDRESS (City, State, and ZIP Code) Hanscom AFB MA 01731-5000
8a. NAME OF FUNDING/SPONSORING ORGANIZATION Rome Air Development Center 8b. OFFICE SYMBOL (If applicable) ESR	9. PROCUREMENT INSTRUMENT IDENTIFICATION NUMBER F19628-85-C-0050
8c. ADDRESS (City, State, and ZIP Code) Hanscom AFB MA 01731-5000	10. SOURCE OF FUNDING NUMBERS PROGRAM ELEMENT NO. 62702F; PROJECT NO. 4600; TASK NO. 20; WORK UNIT ACCESSION NO. 47

11. TITLE (Include Security Classification)
RADIATION HARDENED SILICA-BASED OPTICAL FIBERS

12. PERSONAL AUTHOR(S)
W.J. Miniscalco, T. Wei, P.K. Onorato

13a. TYPE OF REPORT	13b. TIME COVERED	14. DATE OF REPORT (Year, Month, Day)	15. PAGE COUNT
Final	FROM Mar 85 TO Dec 87	December 1988	88

16. SUPPLEMENTARY NOTATION
N/A

17. COSATI CODES			18. SUBJECT TERMS (Continue on reverse if necessary and identify by block number)
FIELD	GROUP	SUB-GROUP	Optical Fibers, Radiation Effects, Glass Structure. (GES)
20	12		

19. ABSTRACT (Continue on reverse if necessary and identify by block number)

Since it is generally recognized that radiation-induced loss is due to pre-existing defects in optical fiber, the technical approaches were designed to reduce the number of these defects in as-drawn fiber and to passivate the ones that remain. While our investigations confirmed that Ce doping leads to greater sensitivity, both the experimental and theoretical results remain ambigous as to whether fluorine is beneficial or deleterious. The diffusion of impurities from the preform substrate tube into the core has been identified as an important source of induced loss. Hydrogen treatment has been found to be an effective means of passivating defects in as-drawn fiber, and improved the hardness of most fibers tested.

20. DISTRIBUTION/AVAILABILITY OF ABSTRACT ☐ UNCLASSIFIED/UNLIMITED ☒ SAME AS RPT. ☐ DTIC USERS	21. ABSTRACT SECURITY CLASSIFICATION UNCLASSIFIED
22a. NAME OF RESPONSIBLE INDIVIDUAL James A. Wall	22b. TELEPHONE (Include Area Code) (617) 377-4031 22c. OFFICE SYMBOL RADC (ESR)

DD Form 1473, JUN 86 *Previous editions are obsolete.* SECURITY CLASSIFICATION OF THIS PAGE

UNCLASSIFIED

TABLE OF CONTENTS

TABLE OF CONTENTS

LIST OF FIGURES

Figure **Page**

LIST OF TABLES

1. INTRODUCTION AND SUMMARY

1.1 OBJECTIVES

The objectives of this program were to determine what influences the sensitivity of multimode optical fiber to radiation and use this knowledge to develop fiber with improved radiation resistance. The effort was directed toward graded index fibers which are required for higher bandwidth applications. Because of the dopants in the core which are required to grade the refractive index, these fibers are much more sensitive to radiation-induced loss than the lower bandwidth, step-index, pure-silica-core fibers.

The program was based upon the well established concept that radiation-induced absorption for the dose levels under consideration [$\leq$25 krad(Si)] is governed by pre-existing defects in the glass [1]. The induced loss is due to color centers which form when existing defects trap the electrons and holes generated by ionizing radiation. The emphasis was on obtaining a fundamental understanding of the relationship between defects in the as-drawn fiber and the glass composition and processing conditions. Using this knowledge, fibers with parameters predicted to be favorable were fabricated and tested.

1.2 TECHNICAL APPROACHES

Induced absorption occurs when existing defects in the glass form color centers by trapping electrons and holes generated by ionizing radiation. The three technical approaches were based upon the principles of reducing the concentrations of these defects or mitigating their effect.

I. Defect Reduction

Reducing the concentration of defects in the as-drawn fiber reduces the amount of color center absorption following irradiation. Common sources of defects are dopants, unintentional impurities, mechanical stress, and thermomechanical stress. Identifying and controlling the major sources of defects accordingly leads to more radiation-resistant fiber.

II. Defect Passivation

One method to prevent defects in as-drawn fiber from capturing charge carriers and thereby forming color centers is to transform them into benign defects. The latter are defined as defects which do not form color centers or which form centers that absorb outside the wavelength range of interest. The passivation process is performed on the residual defects in as-drawn fiber.

III. Recombination Centers

Many defects and impurities have localized electronic states located deep within the fundamental energy gap of the glass. These serve as recombination centers if the states have the ability to trap both electrons and holes. Such centers reduce induced loss if they can compete successfully with other defects for the carriers generated by the radiation.

The program was divided into three phases. In the first or Exploratory Phase all of the three technical approaches were pursued simultaneously. This phase had a duration of $\approx$15 months. The second or Refinement Phase lasted $\approx$10 months during which the activity focused on only the most promising combination of approaches. The final or Optimization Phase involved fine tuning of the successful approaches.

1.3 PROCEDURE

The program involved both an experimental and a theoretical effort. The former consisted of carefully chosen experiments based upon established concepts from the physics of defects in glasses. The primary experimental tool was the measurement of radiation-induced loss in the fibers. This was done both *in situ* at RADC at a fixed wavelength (typically 850 nm), and as postirradiation spectral measurements at GTE Laboratories. More selective techniques such as Raman scattering, photoluminescence, and photobleaching were also employed. These methods have proven to be extremely effective at characterizing defects in fibers. The experimental investigations were supplemented with molecular dynamic simulations of glasses to determine defect types and concentrations. This involved computer generation of glass structures which were then analyzed to identify defects. The objective of the molecular dynamics simulations was to establish the correlation between structural defects and the dopants that were used either to modify the index of refraction or to reduce the defect concentrations.

1.4 SUMMARY OF RESULTS

The defect reduction approach was particularly effective in pointing the direction toward more resistant fiber. Two critical parameters, barrier layer thickness and core dopants, were identified and correlated with radiation-induced loss. Molecular dynamics simulations clarified the role of dopants in producing precursor defects. In addition, the reproducibility with respect to induced loss of both fiber fabrication and measurement was tested and found to be excellent.

Our data indicated that controlling impurities in the fiber plays a more important role in determining radiation sensitivity than controlling the intrinsic defects induced by processing and fabrication. This was determined through the dependence of induced loss on barrier layer thickness which retards the diffusion of impurities from the substrate tube into the core. These conclusions are consistent with the results presented in Interim Report No. 1 [2] and much of the published literature on the subject. It now appears that the precursor defects associated with impurities are more important than isolated native defects. The structure of these defects is not known, but they likely involve complexes of impurities and native defects.

Related to the impurity problem is the increase in radiation sensitivity produced by the index modifying dopants required for graded index fiber. The effects of germanium and fluorine were investigated both experimentally and theoretically. The molecular dynamics simulations were extremely informative with regard to the identification of precursor defects and determining their dependence on dopants. The analyses of computer-generated glasses indicated an increase in defect concentrations as Ge is added to silica which is observed experimentally as increased radiation sensitivity. It also revealed that fluorine codoping has a significant effect upon the defect distribution, decreasing the number of Ge-related defects but increasing the number associated with Si. At present it is not known whether this leads to a more or less favorable distribution of defects, and the experimental results were similarly ambiguous.

The defect passivation approach also yielded encouraging results. Since hydrogen is known to react with defects in fibers, the effects of hydrogen treatment on defect passivation were investigated in detail. Although hydrogen permeation of fiber is generally considered a problem in normal telecommunications applications, we found that it improved the radiation resistance for most of the doped core fibers for which it was tried.

Photoluminescence and photobleaching were found to be extremely effective at detecting and distinguishing defect centers at very low concentrations. These techniques were successful at identifying at least two relevant centers and characterizing their concentrations as a function of fiber treatment and composition. The additional insight these investigations provided into the defect conversion process assisted us in correlating specific centers with radiation-induced loss in the infrared. An interesting result was the detection and photoconversion of defect centers even in untreated, unirradiated fibers. The presence of these centers in as-drawn fibers may also have implications for chemical and photodegradation of optical fibers in nonradiation environments.

The recombination center approach yielded mixed results. Techniques for incorporating Ce into fibers were successfully developed, but the resultant Ge/Ce-codoped fibers had poor radiation resistance. Without developing improved doping procedures for higher purity, lower OH-content fibers, it is not possible to determine whether these results are due to unintentional impurities or are intrinsic to Ce doping. Because of the difficulties and uncertainties associated with this approach, it was abandoned after Exploratory Phase in order to concentrate on the more successful technical approaches.

2. DEFECT REDUCTION APPROACH

The principle underlying the defect reduction approach is to alter the fiber composition, design, or fabrication procedures in order to minimize the number of precursor defects in the as-drawn fiber. The most important step in this approach was the identification of which of the above parameters significantly influence radiation sensitivity. This insight was then applied to the production of harder fiber which was tested and further improved in an iterative cycle.

This technical approach was particularly effective in pointing the direction toward more resistant fiber. Two critical parameters, barrier layer thickness and core dopants, were identified and correlated with radiation-induced loss. However, for any of these investigations to be meaningful, the result must be reproducible. Accordingly, the reproducibility with respect to induced loss of both fiber fabrication and measurement were tested and found to be excellent.

Molecular dynamics simulations were exploited to identify precursor defects and determine their dependence on dopants. This theoretical technique uses the analysis of computer-generated glasses to locate and describe structural defects. The results were very encouraging and it was possible to characterize the increase in defect concentrations as Ge is added to silica. The analysis also indicates that fluorine codoping has a significant effect upon the defect distribution, decreasing the number of Ge-related defects but increasing the number associated with Si.

Our measurements indicated that controlling impurities in the fiber plays a more important role in determining radiation sensitivity than controlling the intrinsic defects induced by processing. These conclusions are consistent with the results presented in Interim Report No. 1 [2] and much of the published literature on the subject. It now appears that precursor defects associated with impurities are more important than native defects introduced by processing and fabrication. The structure of these defects is not known, but they likely involve complexes of impurities and native defects. It is not presently known whether this class of defects is more important because they occur in greater numbers, or have a greater propensity to form color centers, or have a more deleterious location of their absorption bands.

Related to the impurity problem is the increase in radiation sensitivity produced by the index modifying dopants required for graded index fiber. The effects of germanium and fluorine were investigated both experimentally and theoretically through molecular dynamics simulations. Both approaches showed the expected increase in sensitivity with increase in germanium concentration. Moreover, both also gave ambiguous results on the role played by fluorine.

2.1 INVESTIGATIONS OF PROCESS AND DOPING RELATED DEFECTS

2.1.1 Reproducibility of Fiber Drawing and Loss Measurements

In order to examine the consistency of the fiber drawing conditions, irradiation, and loss measurements with respect to radiation-induced loss, additional fibers were drawn from existing preforms and tested. These fibers were then γ-irradiated at RADC to a nominal dose of 20 krad, and the induced losses were compared to those obtained for fibers which had earlier been drawn from the same preforms under identical conditions. The induced loss results are compared at 850, 1000, and 1300 nm in Table 1. In the fiber designation column, the number 1 or 2 indicates the first or second fiber drawing, respectively. The induced losses for two fibers drawn from the same preform are nearly identical except at 1300 nm where the values are too low for accurate measurements.

Previous experiments had established that, within the range investigated, drawing conditions have a relatively minor effect upon radiation hardness [2]. Taken together, these results indicated that preform composition is an important factor influencing radiation sensitivity. Indeed, the induced loss at a given wavelength is virtually the same for all the Ge/F-codoped fibers (HA, LA, and HD). If the results for the three fibers are averaged, one obtains 1.49 ± 0.04 dB/km/krad at 850 nm, 0.33 ± 0.04 dB/km/krad at 1000 nm, and 0.06 ± 0.04 dB/km/krad at 1300 nm. Note that the low dopant fibers (LD) have lower sensitivities at the shorter wavelengths but are identical to the Ge/F-codoped fibers at 1300 nm. The effects of fiber compositions are specifically addressed in Section 2.1.3.

TABLE 1

REPRODUCIBILITY OF RADIATION-INDUCED LOSS MEASUREMENTS

Fiber Designation	Radiation-Induced Loss (dB/km/krad)		
	850 nm	1000 nm	1300 nm
HA-1	1.55	0.30	0.03
HA-2	1.43	0.34	0.12
LA-1	1.51	0.39	0.11
LA-2	1.49	0.29	0.03
HD-1	1.50	0.34	0.05
HD-2	1.48	0.29	0.01
LD-1	1.03	0.24	0.07
LD-2	1.01	0.23	0.06

2.1.2 Barrier Layer Thickness

During the Exploratory Phase we had observed a consistent improvement in radiation hardness of our fibers over the course of time. This favorable but unintentional trend caused us some concern about the reproducibility of the preform fabrication process. One possible explanation was that this was due to a progressive cleanup of the preform fabrication system. If this were an uncontrollable situation or one characterized by "hidden" parameters, it would have serious implications for consistency in fiber production. To test this hypothesis, the composition of the first Ge/F-codoped preform used in the study of drawing parameters was duplicated to determine if the radiation sensitivity could be reproduced. Fiber from the duplicate preform (#860924) was found to have the same radiation-induced loss as that of the original fiber (#851028A). This finding eliminated "cleanup" as the cause of the improvement and verified the consistency of the preform fabrication process.

TABLE 2

EFFECT OF BARRIER LAYER THICKNESS ON RADIATION-INDUCED LOSS

Fiber Designation	# Barrier Passes	Radiation-Induced Loss (dB/km/krad) 850 nm	1000 nm	1300 nm
851028A	10	1.97	0.40	0.06
860924	10	2.10	0.35	0.04
HD	20	1.49	0.32	0.03
MD	20	1.13	0.25	0.04

After tracing the evolution of the fabrication parameters, we concluded that the radiation hardness correlates well with the barrier layer thickness. Table 2 compares the induced loss for fibers with 10 and 20 barrier passes deposited on the inside of the GE Type 982WG fused quartz substrate tube conventionally used in the MCVD process. It is proposed that defect centers responsible for the induced loss are associated with impurities, e.g., alkali ions, which diffuse into the core from the low-purity substrate tube. The impurities must diffuse through the high-purity barrier layer whose thickness is roughly proportional to the number of barrier deposition passes. There is evidence in the literature which suggests that alkali and aluminum ions can diffuse into the fiber core from the substrate tube during the fabrication process [3,4]. Impurities introduced in this way have been shown to increase the radiation sensitivity of Ge-doped fibers [3]. Alkali ions are known to enter the network interstices and generate nonbridging oxygens for charge compensation. Although Figure 1 indicates that a significant reduction in induced loss can be obtained by increasing the barrier thickness, the practical limit for such improvement is not known. In order to determine the asymptotic limit for improving hardness by increasing the barrier thickness, we fabricated a preform using a Suprasil substrate tube which has a very low impurity level. To ascertain a practical barrier layer thickness, two other preforms with five and 20 barrier passes were prepared using GE Type 982 WG substrate tubes. The irradiation and measurement of these fibers are still underway, and the results will be presented at a later date.

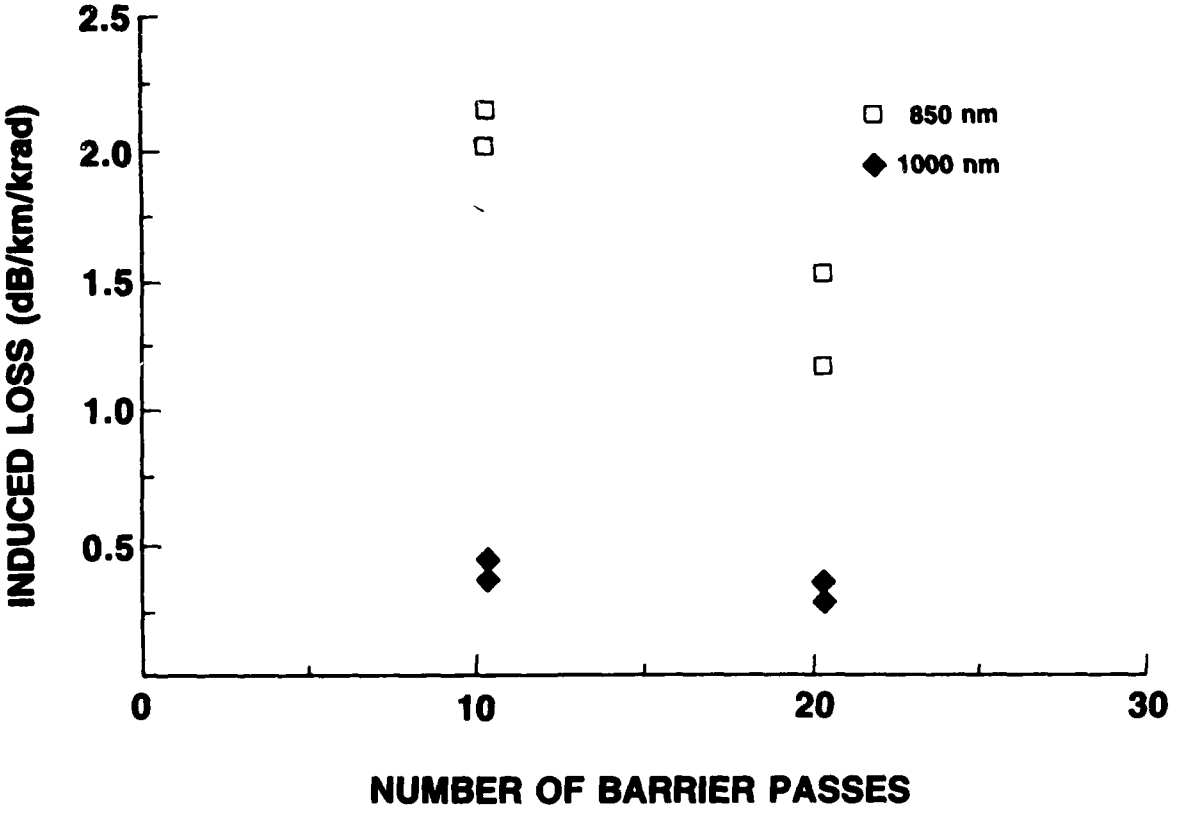

Figure 1: Radiation-induced loss as a function of the number of barrier passes on a fused quartz substrate tube. Losses were measured at 850 and 1000 nm.

2.1.3 Dopant Effects

The preceding discussion of the role played by impurities has a direct bearing on intentional dopants since the latter are expected to produce similar effects. This is well illustrated by phosphorus doping which has an extremely deleterious effect upon long term loss even at long wavelengths. Although phosphorus will substitute for Si in the network, its higher valence must be compensated for by nonbridging oxygens. Since an index modifying dopant is essential to graded index fiber, we have addressed the question of how dopant types and concentrations affect radiation sensitivity. Germanium and fluorine were the dopants included in this investigation. We were particularly interested in studying fluorine as a core dopant because of the controversy surrounding its effects. Gozen *et al.* have observed higher losses for Ge/F-codoped fiber than Ge-doped fiber [5], while Shibata and Nakahara have reported that codoping with fluorine improves radiation resistance [6].

TABLE 3

EFFECTS OF DOPANT TYPES AND CONCENTRATIONS ON RADIATION-INDUCED LOSS

Fiber Design	Core Ge (mole%)	Core F (mole%)	Clad F (mole%)	Radiation-Induced Loss (dB/km/krad) 850 nm	1000 nm	1300 nm
HD	7.6	2.1	2.1	1.49	0.32	0.03
MD	6.5	0.9	2.1	1.13	0.25	0.04
LD	6.7	0	0	1.02	0.24	0.07
861117	7.1	0	0	1.49	0.29	0.06

As part of this investigation, we fabricated four preforms with different Ge and F concentrations in the core, including two without fluorine. Table 3 lists the core and clad dopant concentrations as well as the radiation-induced loss data for these fibers. The results are also illustrated in Figure 2 which indicates the expected trend of increasing induced loss with increasing Ge concentration in the core. However, the trend with F doping is less clear and it is not known if the variations shown are significant or fall within the range of experimental uncertainty. To clarify the role of fluorine doping in radiation sensitivity, additional experiments with different values of concentrations for the two dopants should be conducted.

2.2 MOLECULAR DYNAMICS SIMULATION

2.2.1 Generation of Glass Configurations

Doped silica is significantly more sensitive to radiation than pure silica, implying that doped silica contains higher concentrations of deleterious precursor defects. Although there has been some experimental and theoretical success at identifying these defects, the description remains incomplete and largely unquantitative. In particular, the experimental techniques measure only average properties and defect structures must be largely

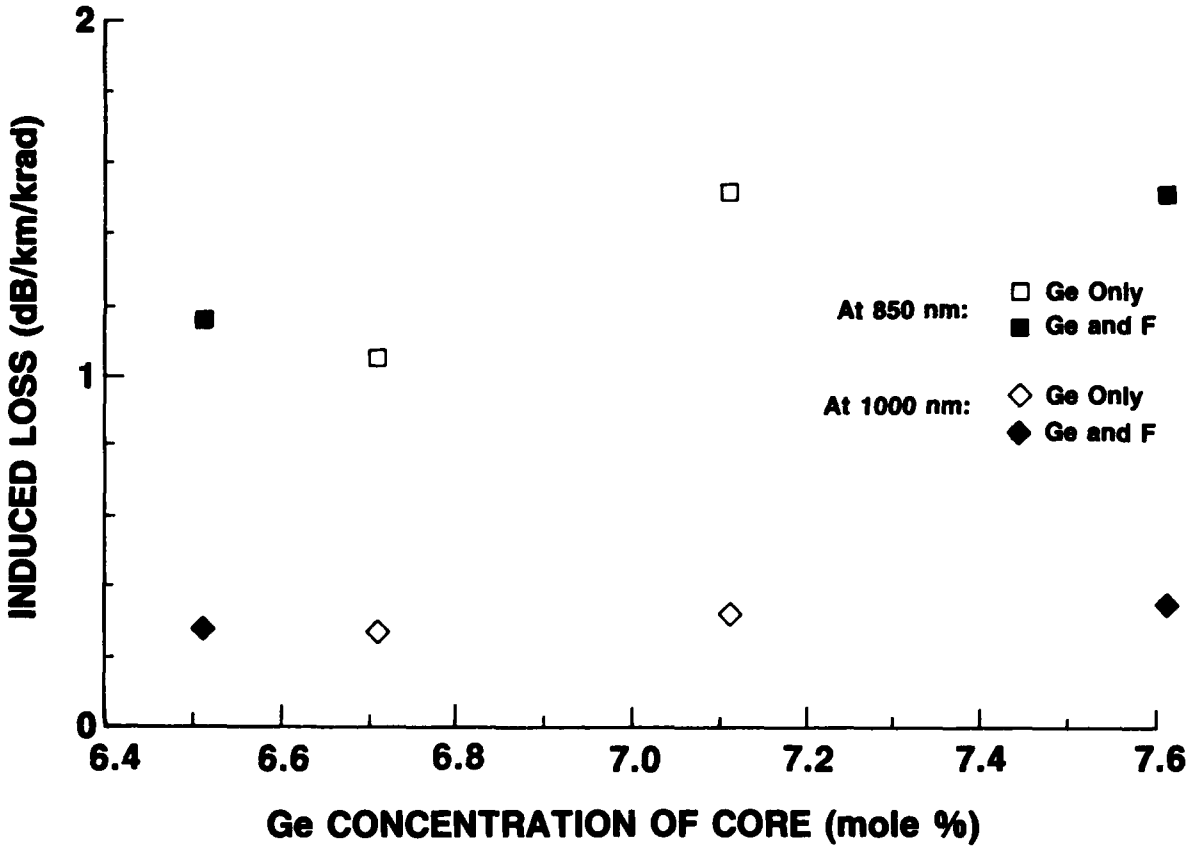

Figure 2: Radiation-induced loss as a function of the Ge concentration of the fiber core. Losses were measured at 850 and 1000 nm. Empty symbols are fibers doped only with Ge in the core; filled symbols are fibers codoped with both Ge and F in the core.

inferred. To obtain a more complete inventory of the types and concentrations of structural defects which result from the incorporation of standard index modifying dopants, we have analyzed computer-generated glasses produced using molecular dynamics. It is expected that among these structural defects are those which, when irradiated, will form color centers absorbing at wavelengths of importance. Molecular dynamics generates a glass by calculating the pairwise interionic forces of a large array of ions. The net force on each ion is then used to determine its velocity and position slightly later in time. The new positions are in turn used to recalculate the interionic forces. This process is iterated until an equilibrated structure (i.e., one whose average properties no longer change with time) is reached. The equilibration temperature is 6000 K which gives the ions considerable mobility and results in thorough mixing in a very short period of time. After equilibration, the

glass is cooled to room temperature by removing kinetic energy in several steps, i.e. slowing the ions.

The primary shortcoming of a molecular dynamics simulation in this application is its inability to treat the electrons in the system. The constituents are necessarily assumed to be ions and consequently covalent bonds cannot be reproduced. This leads to a degree of arbitrariness in the definition of a bond. Moreover, certain covalent defects such as Si – Si bonds and peroxyl bridges (–O–O–) are not expected to be accurately predicted. A lesser problem is that the high temperature (6000 K) from which the glass is quenched is expected to overestimate the defect concentration. This difficulty is addressed by cooling the glass in steps to several intermediate temperatures at which it is allowed to further equilibrate. Overall, molecular dynamics simulations have been shown to accurately reproduce experimentally verifiable features of the glass structure such as radial distribution functions. The general trends in defect types and concentrations, as well as the structure of many specific defects, are expected to be accurately represented.

The program used to generate the glasses requires empirical parameters which characterize the interionic forces for each of the species. These parameters are chosen by adjusting their values until the average interionic distances agree with experimental values. The array is limited to 180 ions to make the computational problem tractable. Because of the small sample size, accurate statistics are obtained using multiple configurations of the same basic cell. After the glass has equilibrated, it is quenched to room temperature to form the first configuration. The glass is then allowed to further evolve at room temperature. After a specified number of steps the structure of the glass is saved as another configuration. For the pure SiO_2 and GeO_2, two quenches separated by 2 ps at high temperature were performed. Each of the quenches was used to generate 500 room temperature configurations. For glasses with only one type of dopant ion, 10 cooling runs were done and 100 room temperature configurations from each were saved, again for a total of 1000. In glasses with two types of dopants, 14 quenches were performed and 100 room temperature configurations saved for each, for a total of 1400 configurations to be analyzed. The location of each ion in each configuration was saved and separate computer programs were used to analyze the structure.

The analysis programs calculate the radial distribution function (RDF) of each type of ion pair, the probability of various types of bonds and nearest neighbors, and the distribution of intra- and inter-tetrahedral bond angles. The RDF is the average number of ions per

unit volume of a particular type as a function of distance from a specified kind of ion. A classification scheme for normal and abnormal bonds was defined and is explained below. An intra-tetrahedral angle is the angle between the vectors from a cation to any two anions of the same tetrahedron. Inter-tetrahedral angles are formed by the intersection of the vectors from an anion shared by two tetrahedra and the cations at the center of those tetrahedra. Additional conditions may be applied in the above analyses, for example, to differentiate ions near a dopant ion from those which have no dopant ion within a given distance.

Five glass compositions were generated and analyzed. They are pure SiO_2, pure GeO_2, SiO_2 doped with 10 mole% GeO_2 (G6S54), SiO_2 doped with 10 mole% GeO_2 and 5 anion% fluorine (F6G6), and SiO_2 doped with 5 anion% fluorine (SiF6). The compositions of the five glasses on an ionic basis are shown in Table 4.

TABLE 4

COMPOSITIONS OF GLASSES ON AN IONIC BASIS

Glass	Number of Ions			
	Si	Ge	O	F
SiO_2	60	0	120	0
GeO_2	0	60	120	0
Ge-doped (G6S54)	54	6	120	0
F-doped (SiF6)	59	0	115	6
Ge/F-doped (F6G6)	53	6	115	6

2.2.2 Radial Distribution Functions

In considering the variety of structural unit possible in glasses, it was recognized that the definition of "bond length" or "broken bond" using an ionic potential is arbitrary. Therefore, on the basis of the RDFs we have defined "normal bonds" (–), "stretched bonds" (- -), and "no bonds" as shown in Table 5. The same definitions are applied to all glass compositions.

TABLE 5

DEFINITIONS OF NORMAL AND STRETCHED BONDS

Bond Type	Bond Length (nm)		
	Normal	Stretched	No Bond
Si – O	0.140 – 0.173	0.173 – 0.200	> 0.200
Ge – O	0.160 – 0.189	0.189 – 0.209	> 0.209
Si – F	0.145 – 0.163	0.163 – 0.191	> 0.191
Ge – F	0.160 – 0.183	0.187 – 0.209	> 0.209

The Si – O RDFs for the analyzed Si-containing glasses are shown in Figure 3. The average Si – O bond length is longer in the doped glasses than in pure silica. The unrestricted Si – O RDFs (i.e., for all Si ions) for the Ge-doped and the Ge/F doped glasses are virtually identical, and only the latter is shown. For the doped glasses there are, however, restricted RDFs (i.e., subject to some condition) that are radically different. This is illustrated in Figure 3 for the Ge/F doped glass: the Si – O RDF calculated subject to the condition that the Si ions have a normal bond to a fluorine is compared to that for Si ions with a stretched bond to a fluorine. The most probable Si – O bond length for Si ions that also form normal Si – F bonds is the same as that of pure SiO_2. However, these Si ions form fewer longer than average Si – O bonds than pure SiO_2, indicating that SiO_3F tetrahedra are tightly bound. This is not surprising since this complex has excess positive charge and less repulsion among the anions. The Si – O RDF for Si ions that form stretched Si – F bonds shows a wide distribution of bond lengths, indicating a variety of Si coordinations. The distribution of structural units formed by Si will be described below.

Figure 4 compares the unrestricted Si – O RDF for pure silica to those of the doped glasses calculated subject to the restrictions that the O ion be normally bonded to Ge and that O not be bonded to Ge. When an oxygen ion forms a bridge between Si and Ge, both the Si – O bond and the Ge – O bond are compressed relative to their unrestricted most probable lengths in the Ge-doped glass and pure germania, respectively. This is because of the large size of the Ge ion compared to Si. However, the repulsion factor in the potential is such a strong a function of separation [$\alpha \exp(-r/.029)$] that the Si – O distance cannot be compressed to significantly less than that observed in pure silica. For the Ge-doped glass, the average Si – O distance for oxygens that are not bonded to Ge actually

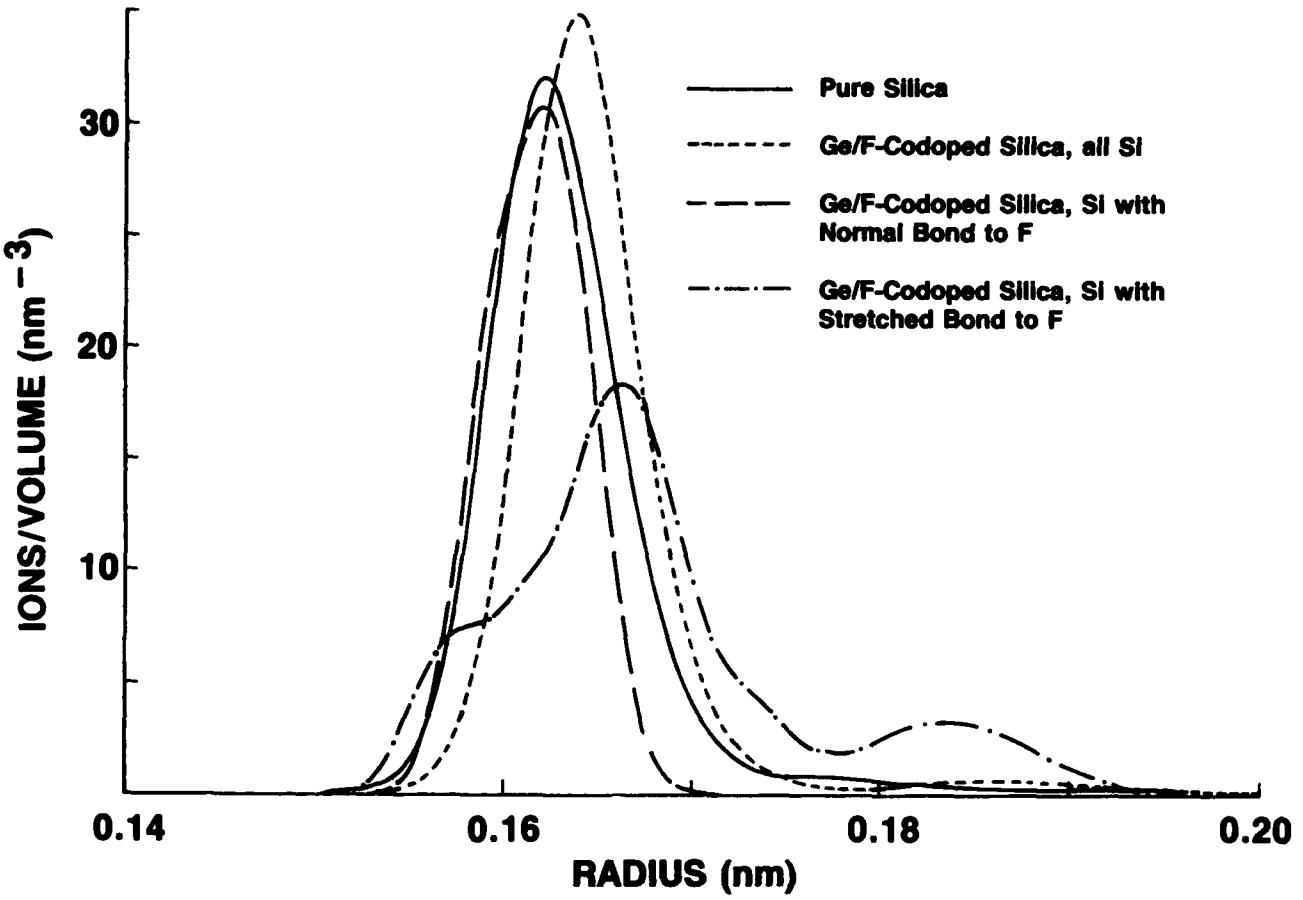

Figure 3: Si – O radial distribution functions for pure silica and Ge/F-codoped silica. The unrestricted RDF for Ge-doped silica is indistinguishable from that of the codoped glass.

increases. This is reflected in an increase in the fraction of stretched Si – O bonds, but not in the fraction of non-bridging oxygens (NBOs), which is zero in the doped glasses.

Examining the Ge – O RDF (Figure 5), the most probable Ge – O distance is smaller in the doped glass than in pure GeO_2. This agrees very well with EXAFS and x-ray scattering measurements of the Ge – O distance in GeO_2-doped SiO_2 [7]. The Ge – O bond is expected to be compressed toward the value of the Si – O bond in the smaller silica matrix. However, the distribution shows no Ge – O bonds shorter than that observed in pure GeO_2, reflecting the exponential dependence on distance of the repulsion factor. The RDFs of both GeO_2 and Ge-doped SiO_2 have a significant density of oxygens at a distance greater than 0.19 nm from Ge. These are too long to be considered normal bonds.

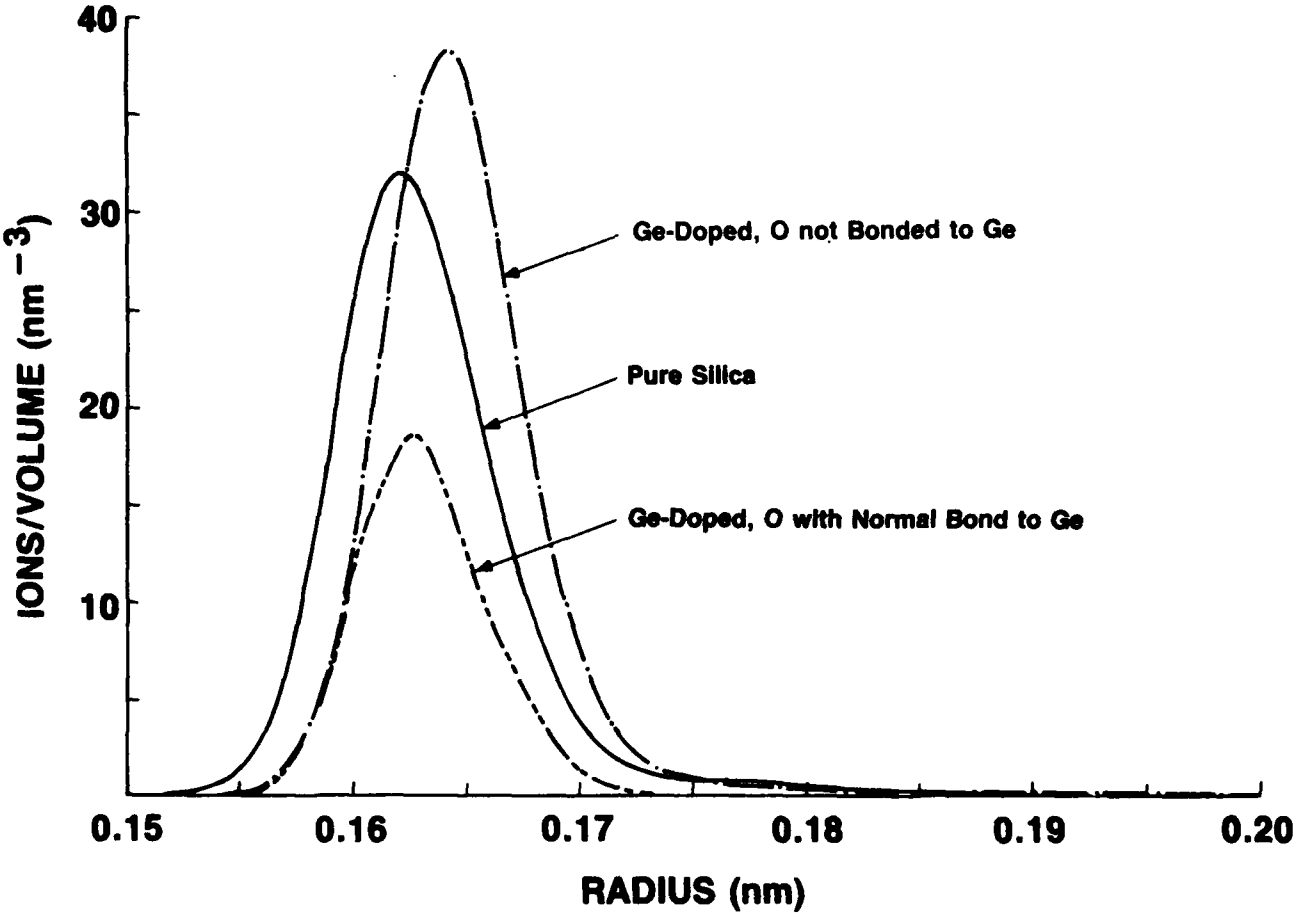

Figure 4: The unrestricted Si – O radial distribution function for pure silica compared to those of the Ge-doped glass calculated subject to the restrictions that the O ion be normally bonded to Ge and that O not be bonded to Ge. See Table 5 for bond length definitions.

When fluorine is added to the Ge-doped glass (composition F6G6), the long distance tail of the Ge – O RDF disappears, even though the Ge – O bond distance for Ge ions also bonded to F is greater than the average bond length for all Ge ions in any of the Ge-containing glasses (Figure 5). The Ge – F RDF itself is quite interesting (Figure 6), showing two distinct classes of Ge – F bonds. By examining the nearest neighbors for Ge ions in each class of Ge – F bonds, it was found that the fluorine ions that form a normal bond (Table 5) with Ge are terminal or nonbridging F ions. Fluorine ions that form a stretched bond with Ge are bridging and form a Ge - - F – Si unit. The Ge – O RDFs for Ge ions in either Ge – F class are identical (Figure 5) because they are largely the same Ge ions. Nearly 90% of the Ge ions bonded to one or more F ions are, in fact, bonded to two fluo-

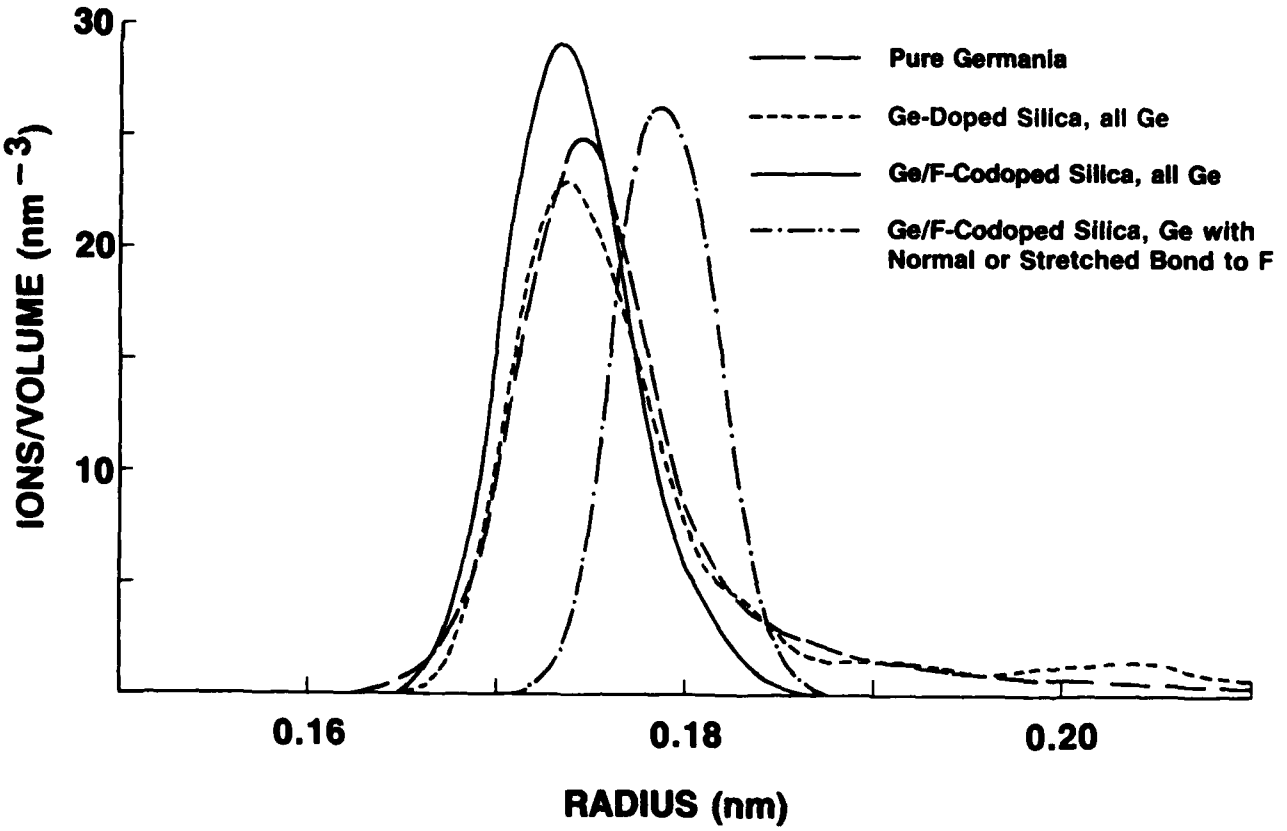

Figure 5: Unrestricted Ge – O radial distribution function for pure germania compared to those of the Ge-containing glasses.

rines through one normal and one stretched bond (F – Ge - - F). An additional 7% have normal bonds to two fluorines, leaving only 3% bonded to a single F ion. Overall, 16.66% of all Ge ions are bonded to one or more F ions, and 16.18% are bonded to two F ions. This indicates a high affinity between Ge and F since only 1.16% of the Ge ions would be bonded to two fluorines if the Ge and F ions were randomly distributed throughout the network. All Ge ions that form at least one Ge – F bond are also bonded to three oxygens and all Ge ions that are not bonded to any F ions (83.3% of the Ge ions) are bonded through normal bonds to four oxygen ions. Therefore, approximately 84% of the Ge ions are 4-coordinated and 16% of the Ge ions are 5-coordinated with two of the neighbors being F ions.

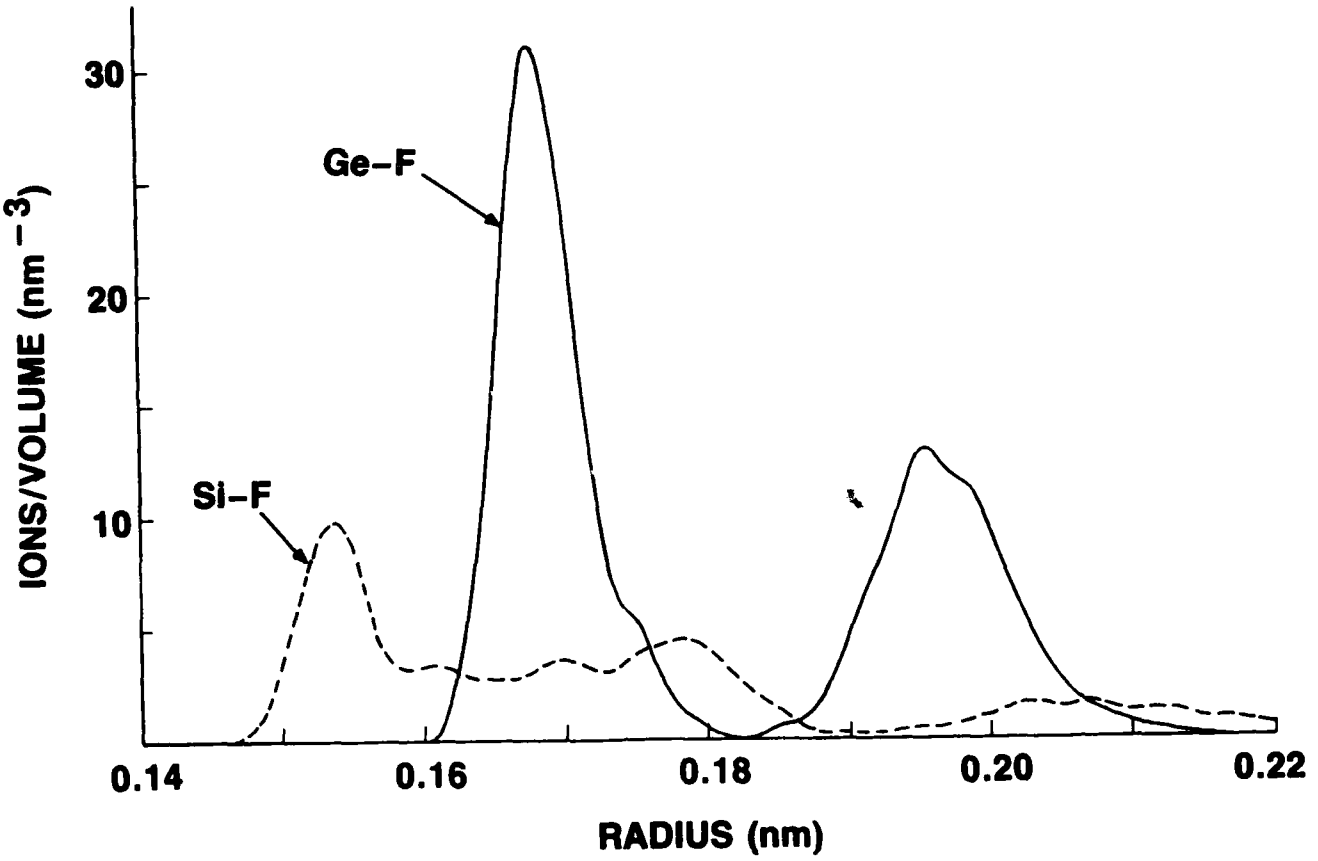

Figure 6: Si – F and Ge – F radial distribution functions for Ge/F-codoped silica.

The effect of fluorine on the Si coordination in the codoped glass is even more complicated. Ten different types of Si structural units were found in significant amounts. These are illustrated in Figure 7 along with the fraction of Si ions found in each category. The analysis indicates that 93.09% of the Si ions are 4-coordinated, some including one F ion; 6.82% of the Si ions are 5-coordinated, again with some including one F ion; and 0.09% of the Si ions are only 3-coordinated. The latter complexes may be precursors to E' centers which would form if a 3-coordinated Si trapped an electron at the site of the "missing" oxygen. The 5-coordinated silicons may be the simulation's attempt to produce the peroxyl bridge which cannot actually be generated by a calculation using ionic potentials.

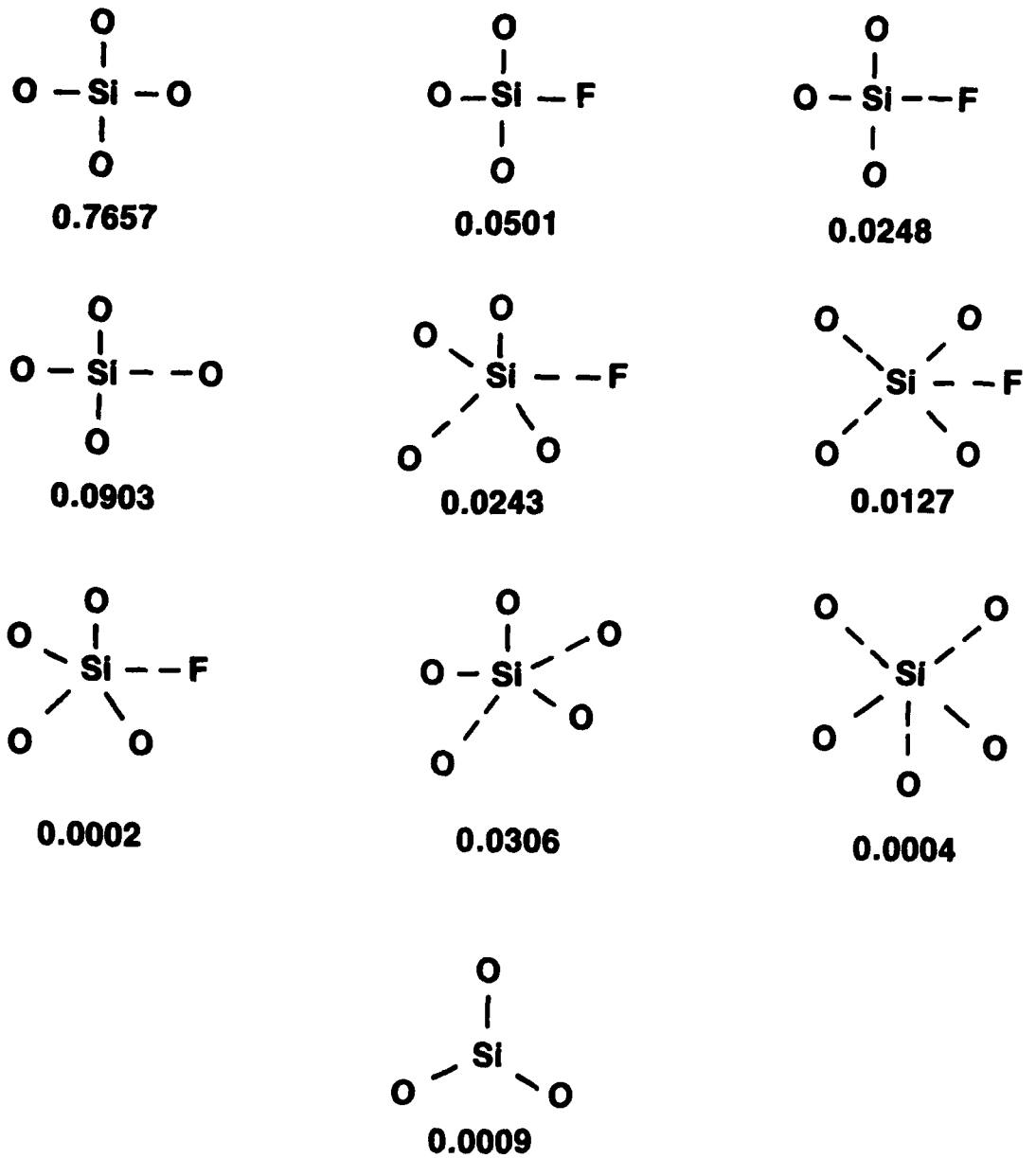

Figure 7: The types of Si structural units generated by molecular dynamics simulation showing the fraction of Si ions found in each category. Normal bond: — ; stretched bond: - - .

2.2.3 Anion Environments

The coordination of the anions was examined in detail for the four analyzed glasses. The fraction of oxygens or fluorines forming each observed structural unit is shown in Tables 6 and 7. Even in pure SiO_2 a number of defects are observed, including stretched bonds, 3-coordinated oxygens, and NBOs. The latter are precursors to the nonbridging oxygen hole center which forms when the NBO traps a hole. The 3-coordinated and 1-coordinated oxygens may represent an ionic approximation to valence alternation pairs. Pure GeO_2 has a significantly larger fraction of abnormal and missing bonds than either SiO_2 or the doped glasses. This implies that the GeO_2 complex itself has more defects than the SiO_2 complex, and the observed radiation sensitivity may not be merely a consequence of mixing but intrinsic to Ge-containing glasses.

These defects are more complicated than just non-bridging oxygens, for the fraction of NBOs in GeO_2 is actually less than in pure SiO_2, and none at all are found in the simulations of the doped glasses. The fraction of oxygens that form one normal and one stretched bond is comparable in the two pure glasses and is somewhat decreased in the doped glasses. The fraction of oxygens which form two stretched bonds is small in all glasses. The most significant difference in defect structure among the glasses is found in the total number of 3-coordinated oxygens. In pure SiO_2, only 1.03% of the oxygens are in 3-fold coordination, while for pure GeO_2 the number is 5.48%. In the doped glasses, with only 10 mole% GeO_2, the fraction of oxygens in 3-fold coordination is more than twice as great as in pure SiO_2 (2.22% in G6S54 and 2.28% in F6G6). Viewing the glass as corner-connected SiO_4 or GeO_4 tetrahedra, one concludes that at least two stretched Si – O bonds or at least one stretched Ge – O bond is needed to form a 3-coordinated oxygen. Garofalini has reported finding 3-coordinated oxygens in a molecular dynamics simulation of pure silica, and he also observed that these are associated with stretched Si – O bonds [8]. A 3-coordinated oxygen cannot be shared by three regular tetrahedra; they must be distorted. For the codoped glass (F6G6), the addition of fluorine eliminates 3-coordinated oxygens bonded to Ge (Table 7), as well as all stretched Ge – O bonds. The latter is reflected in the Ge – O RDF in Figure 5. However, the total number of 3-coordinated oxygens does not decrease significantly because of an increase in the number of oxygens coordinated by three silicons (Table 7). The effect of fluorine doping on radiation sensitivity is complex: it alters the types but not the total numbers of 3-coordinated oxygens. This ambiguity is reflected in the experimental measurements of radiation-induced loss.

TABLE 6

FRACTIONS OF 1- AND 2-COORDINATED OXYGENS

Coordination	SiO_2	GeO_2	G6S54	F6G6
Si–O	0.0042	0	0	0
Ge–O	0	0.0019	0	0
Si–O–Si	0.9342	0	0.7808	0.7702
Ge–O–Ge	0	0.8912	0.0186	0.0261
Si–O–Ge	0	0	0.1394	0.1478
Si–O--Si	0.0489	0	0.0282	0.0322
Si–O--Ge	0	0	0.0077	0
Ge–O--Ge	0	0.0513	0.0005	0
Ge–O--Si	0	0	0.0001	0
Si--O--Si	0.0012	0	0.0017	0.0008
Si--O--Ge	0	0	0.001	0
Ge--O--Ge	0	0.0001	0	0

TABLE 7

FRACTIONS OF 3-COORDINATED OXYGENS

Coordination	SiO_2	GeO_2	G6S54	F6G6
Ge–O(Ge)(Ge)	0	0.0092	0.0010	0
Si–O(Si)(Si)	0.0049	0	0.0045	0.0090
Si–O(Ge)(Ge)	0	0	0.0027	0
Ge–O(Ge)(Ge)	0	0.0385	0.0044	0
Si–O(Si)(Si)	0.0064	0	0.0082	0.0138
Ge–O(Si)(Si)	0	0	0.0013	0
Ge–O(Ge)(Ge)	0	0.0071	0.0040	0

When the fluorine coordination was examined, eight varieties of fluorine-containing structural units were found. There are no bridging fluorine ions with two normal bonds; nor are there any 3-coordinated fluorine ions. Although only 10% of the cations are Ge, 25% of the Cation – F bonds are formed with Ge. Thus there is a preference for F to bond with Ge.

2.2.4 Intra-tetrahedral Bond Angles

The intra-tetrahedral bond angles were calculated using the actual Cation – O and O – O distances for the ions forming a tetrahedron. The distributions were determined by calculating the bond angles for all the cations in all the glass configurations. Since the potential does not include any 3-body interactions or directional forces, the results are dominated by packing considerations and the ionic repulsion term. Given these limitations, the distribution of angles is not expected to be quantitative for a covalent material, but rather to provide an indication of what is possible in the real glasses. The unrestricted O – Si – O bond angle distributions are shown for the three silica glasses in Figure 8. The distributions are very broad, from 85 to 150 degrees, with maxima ranging from 103 to 110 degrees, and little sensitivity to composition. This shows that the SiO_4 tetrahedral angles are, in general, well defined. However, if we focus on the O – Si – O bond angles formed by Si ions that are also bonded to F through a stretched Si – F bond (Figure 9), the distributions change dramatically. The structural units included in this distribution are both 4- and 5-coordinated, as depicted in Figure 7. Thus fluorine has thoroughly distorted some of the tetrahedra.

If we compare the O – Ge – O bond angle distributions in the three Ge-containing glasses for normal Ge – O bonds (Figure 10), we find that there is a strong dependence on composition and the distribution in the doped glasses is more irregular than in pure GeO_2. Thus the Ge-doped glass is not just a mixture of GeO_4 and SiO_4 tetrahedra, but the GeO_4 tetrahedra are distorted by their surroundings in the SiO_2 network. When only Ge ions that form Ge – F bonds are examined (Figure 11), the distributions are considerably narrower and two sharp peaks are found. In most of these structural units, the Ge ions are 5-coordinated and the stretched Ge – O bonds have been eliminated. Assuming a Ge – O distance of 0.174 nm, the peak at 88 degrees corresponds to an O – O distance of 0.242 nm and the peak at 152 degrees corresponds to an O – O distance of 0.341 nm.

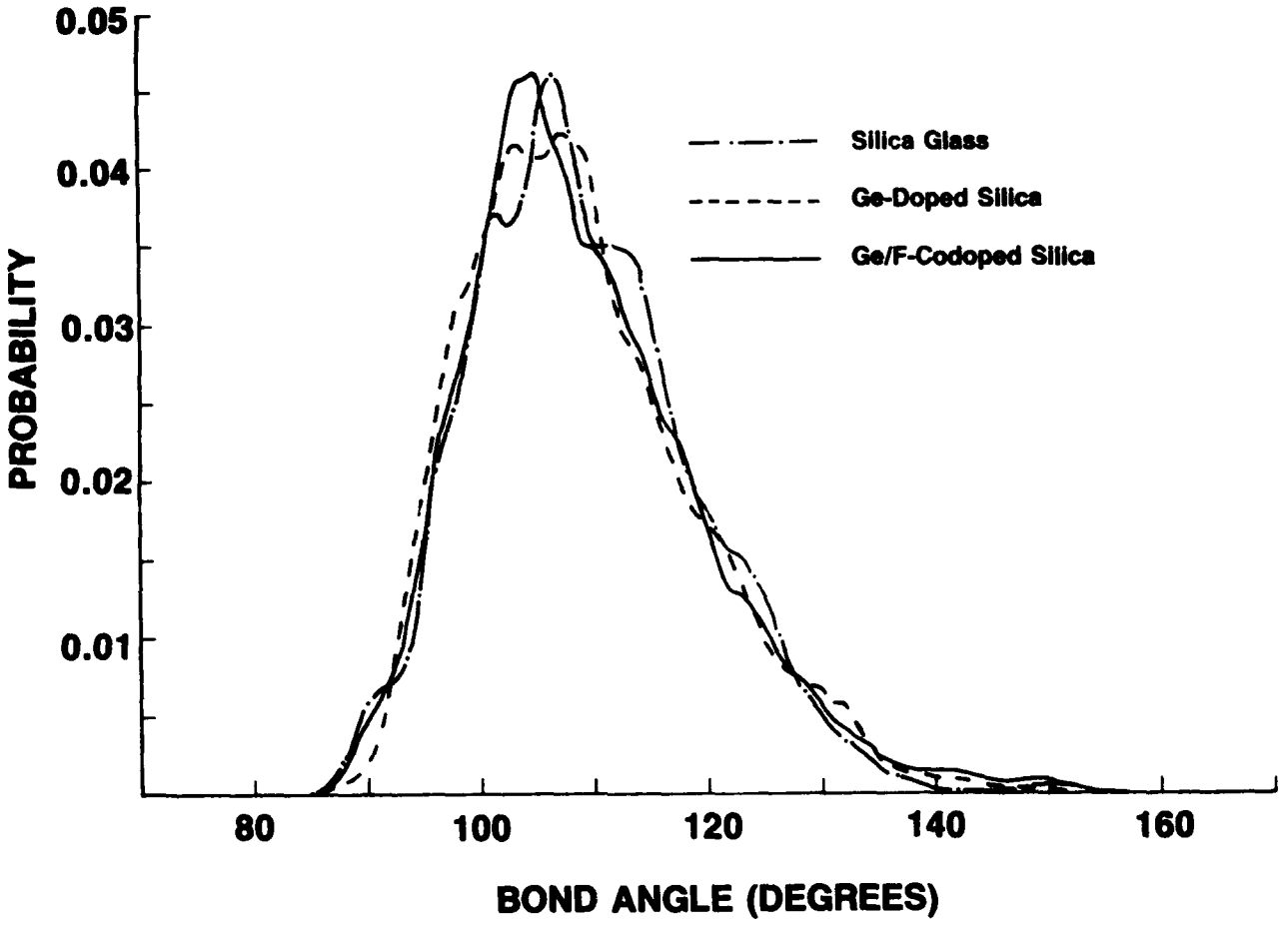

Figure 8: Comparison of the unrestricted O – Si – O bond angle distributions for pure, Ge-doped, and Ge/F-codoped silica.

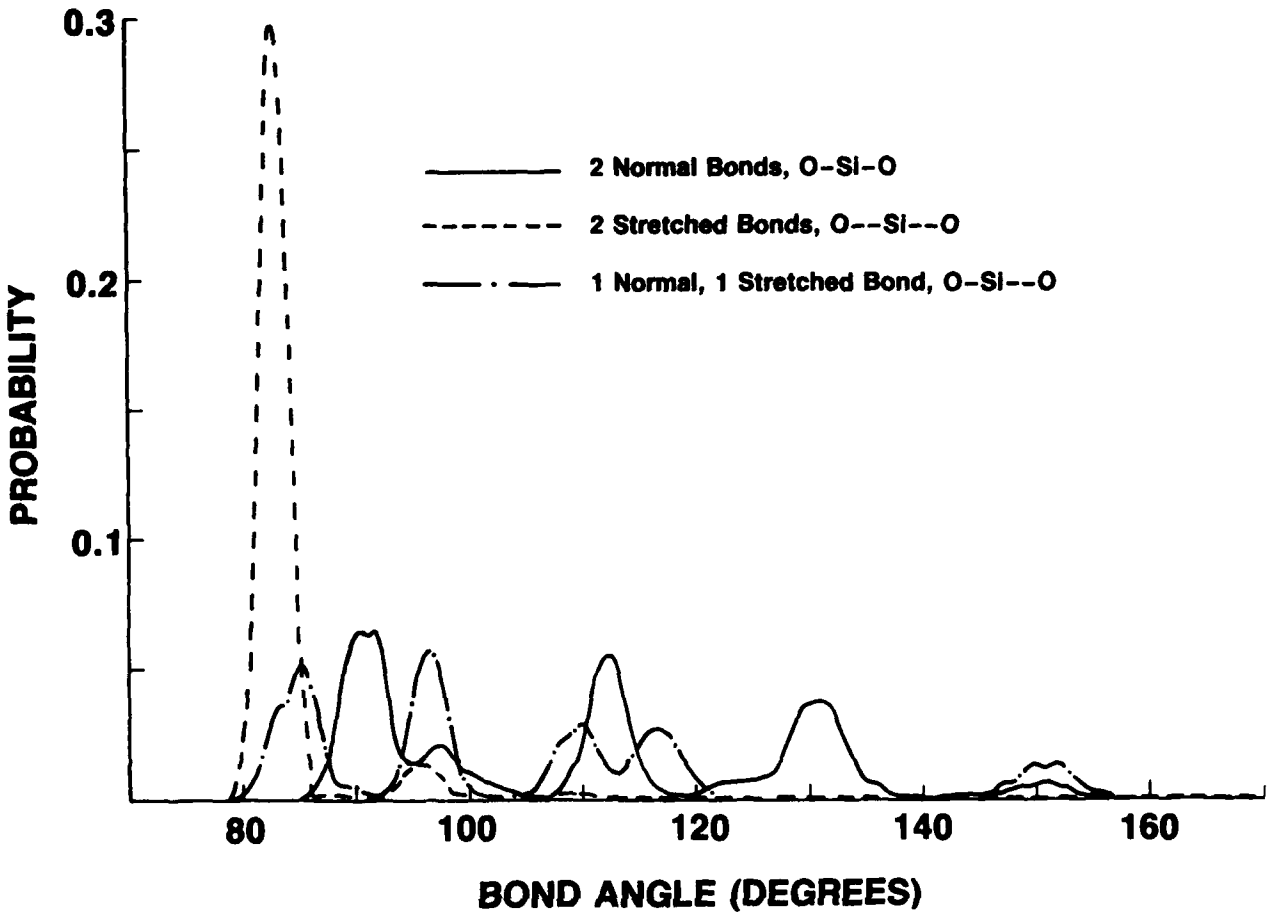

Figure 9: The O – Si – O bond angle distributions for Si ions in the Ge/F-codoped silica that are also bonded to F through a stretched Si – F bond. Curves are for different categories of Si – O bonds. See Table 5 for bond length definitions.

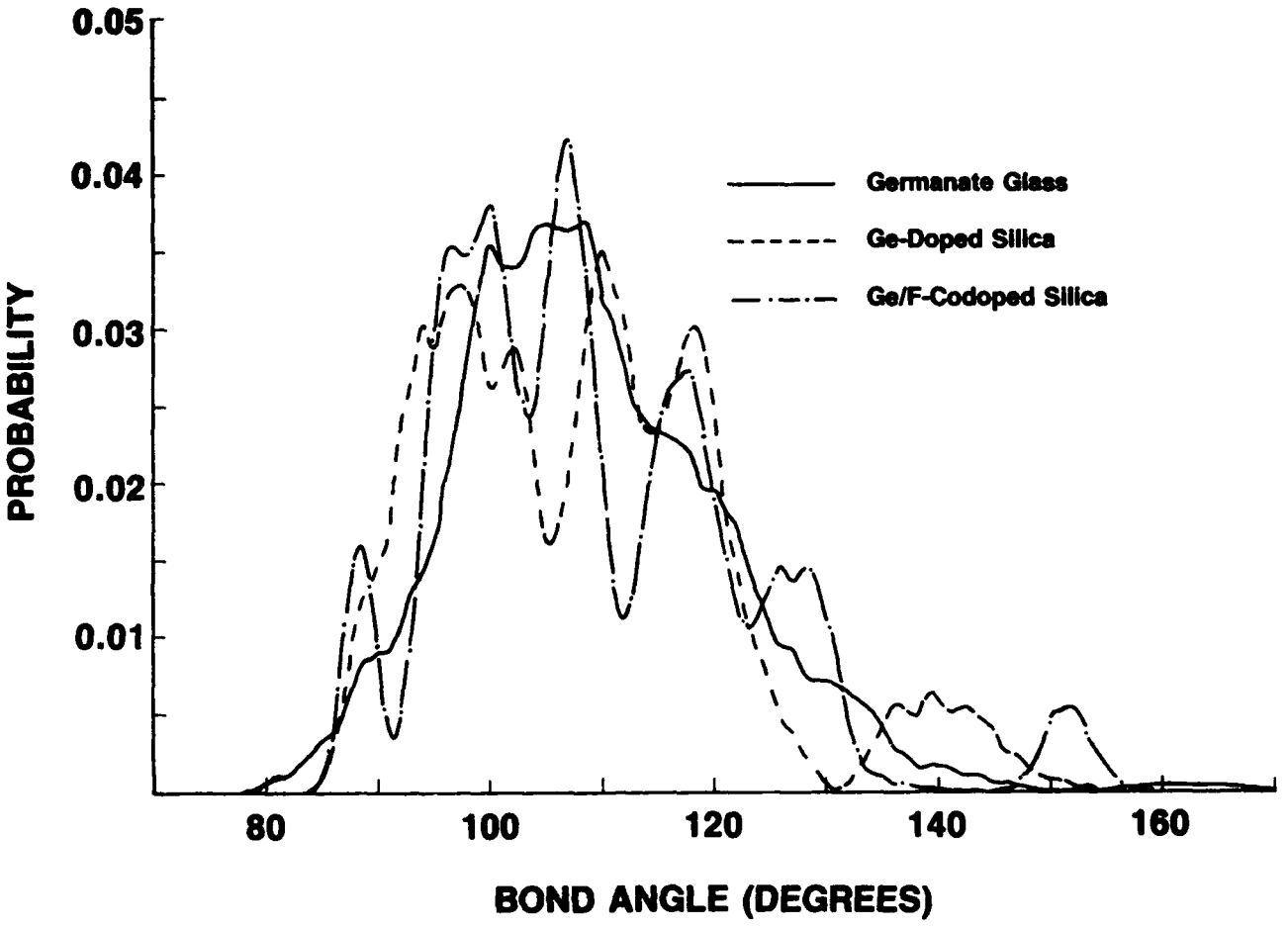

Figure 10: Comparison of O – Ge – O bond angle distributions for pure germania, Ge-doped silica, and Ge/F-codoped silica subject to the restriction of normal Ge – O bonds. See Table 5 for bond length definitions.

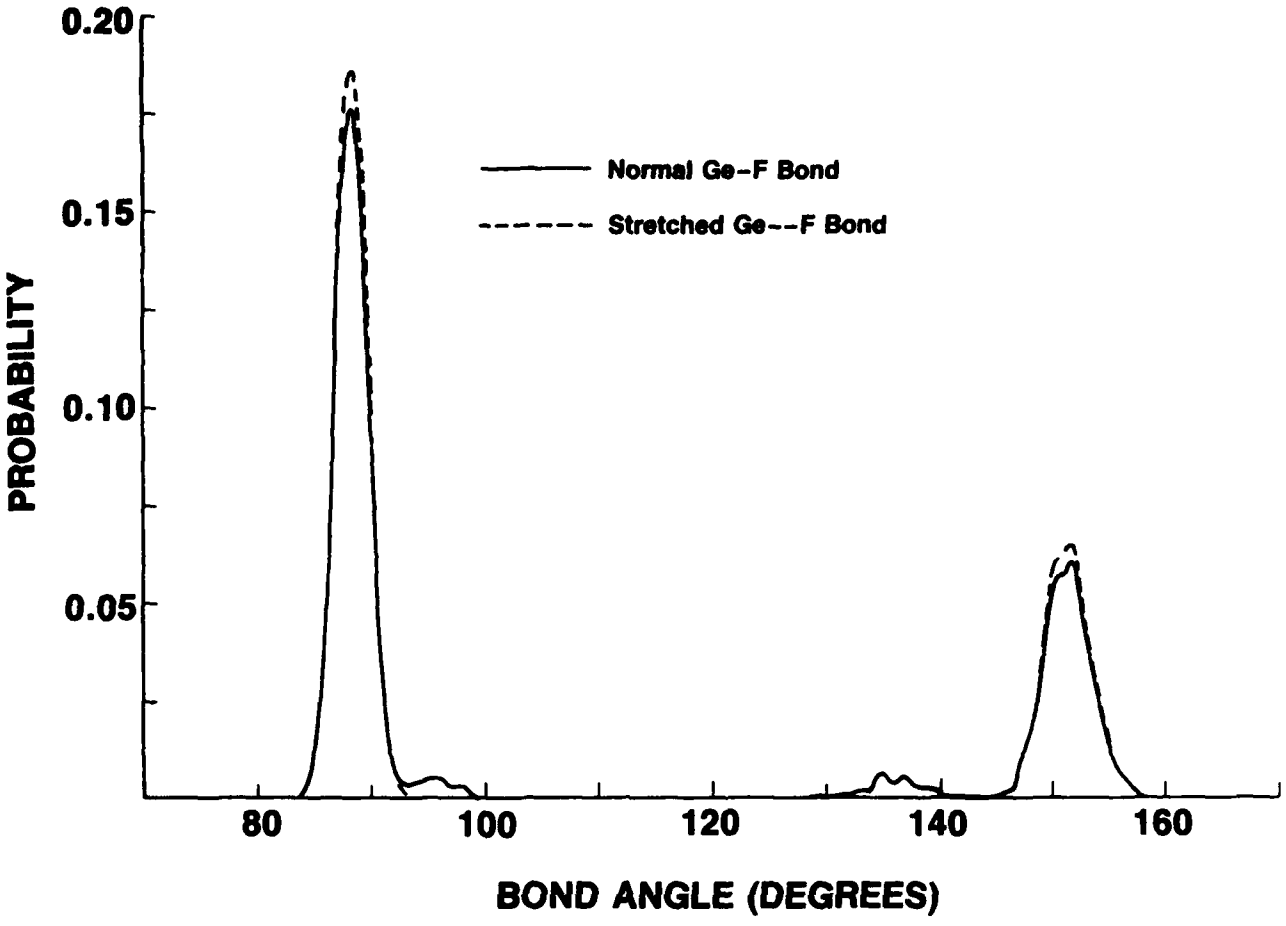

Figure 11: O – Ge – O bond angle distributions for Ge ions bonded to F in Ge/F-codoped silica. Curves are for normal and stretched Ge – F bond lengths. See Table 5 for bond length definitions.

3. DEFECT PASSIVATION APPROACH

The concept underlying the defect passivation approach is that of converting the residual deleterious precursor defects in as-drawn fiber into more benign defects. The latter are defects which, when irradiated, do not form color centers with significant absorption in the spectral region of interest. Since hydrogen is known to react with defects in fibers, the effects of hydrogen treatment on defect passivation were investigated in detail. Although hydrogen permeation of fiber is generally considered a problem in normal telecommunications applications, we found that it improved the radiation resistance of most of the doped-core fibers for which it was tried.

In conjunction with this technical approach we undertook a series of photoluminescence, Raman scattering, and photoconversion/photobleaching investigations. These techniques are extremely effective at detecting and distinguishing defect centers at very low concentrations. The investigations were successful at identifying at least two relevant centers and characterizing their concentrations as a function of fiber treatment and composition. An interesting result was the detection and photoconversion of defect centers in even untreated, unirradiated fibers. The presence of these centers in as-drawn fibers may also have implications for chemical and photodegradation of optical fibers.

3.1 HYDROGEN TREATMENT

The effectiveness of the defect passivation approach in reducing radiation-induced loss for Ge/P-codoped fibers through the use of hydrogen treatment had been previously demonstrated (see Section 2.1 of Interim Report No. 1 [2] and Appendices A and B) [9,10]. It was found that a fiber pretreated with hydrogen had only half the induced loss at 1 μm as that of an untreated fiber. To evaluate the effectiveness of hydrogen treatment for fibers with greater radiation resistance, two Ge/F-codoped fibers from the core-clad interfacial stress study were chosen. Details on the design and fabrication of these fibers (designated HA and LA) are found in Section 3.3 of Interim Report No. 1 [2]. Sections of fibers HA and LA were treated in 4 atm hydrogen at 50°C for 10 days. Afterwards the fibers were left in air at room temperature until the unreacted hydrogen diffused out, and then irradiated to a

total dose of 18 krad. Table 8 summarizes the induced loss results for fibers with and without hydrogen treatment. The treated fibers show a 14% improvement in radiation resistance at 850 nm over untreated fibers. However, for the hardest fiber (fiber LD) no improvement was observed.

TABLE 8

RADIATION-INDUCED LOSS FOR HYDROGEN TREATED AND UNTREATED FIBERS

Fiber Designation	Hydrogen Treatment	Radiation-Induced Loss (dB/km/krad) 850 nm	1000 nm	1300 nm
HA	No	1.49	0.32	0.08
HA	Yes	1.28	0.33	0.08
LA	No	1.50	0.34	0.07
LA	Yes	1.29	0.30	0.04

On the basis of these results we conclude that the defect passivation approach yields significant improvement in radiation resistance even for relatively hard doped-core fibers. The very hardest fibers, however, benefit little from hydrogen treatment. Problems with increased hydroxyl absorption can be eliminated through the use of deuterium rather than hydrogen. However, we have observed that the hydrogen treatment of high purity, low-defect-level fiber results in very little increase in hydroxyl concentration and the use of deuterium may not be necessary. This variability in the degree to which hydrogen reacts to form hydroxyl groups in fibers is an important issue in its own right, and might be exploited as a means to measure defect concentrations.

3.2 PHOTOLUMINESCENCE AND PHOTOBLEACHING

Radiation-induced loss measurements, which were the primary characterization tool used in this program, are generally not selective enough to identify the specific centers which are responsible for the absorption. In addition, analysis of glasses generated by molecular dynamics simulation reveals defects which occur at too low a concentration to be detected by the standard structural analysis techniques such as x-ray diffraction, EXAFS, and neutron diffraction. In order to obtain the required sensitivity and selectivity, we have turned to Raman scattering and photoluminescence in fibers. These techniques were augmented by photobleaching, a process which involves the photoconversion of one type of defect into another. This selective approach was used to identify specific color centers and precursor defects, as well as to correlate their concentrations with preform composition and fiber processing. Photoluminescence was found to be a very sensitive probe of defect centers. Significant differences were found for the same fiber subjected to different treatments and for different fiber compositions subjected to the same treatment.

3.2.1 Procedure

The general procedure was to first examine the color center luminescence excited for a range of laser wavelengths, λ_{ex}. These measurements were performed at low power to minimize photobleaching. The fibers were then subjected to an intense photobleach using a wavelength in the range 470 – 490 nm, and the photoluminescence spectra remeasured to determine the changes in defect center concentrations. To make absolute comparisons of the intensities, the emission spectra were scaled by equalizing the intensities of the Raman scattering for the different fibers. In the analyses reported here, Si – O vibrational lines were used for this normalization.

The photoluminescence investigation was applied to Ge/P- and Ge/F-codoped fibers. The results for the Ge/P-codoped fibers were included in Section 3.2 of Interim Report No. 1 [2]. These observations will be reviewed and a more recent study of the Ge/F-codoped fibers will be presented along with a comparison of the results for the two fiber compositions.

The three Ge/P-codoped fibers were drawn from the same preform. The samples were short ($\leq$ 3 m) sections taken from the fibers discussed in Section 2.1 of Interim Report No. 1. These were (1) a pristine as-drawn fiber, (2) a fiber which was irradiated to 4.6 krad

without pretreatment, and (3) a fiber which was hydrogen treated and then irradiated to 4.5 krad. The hydrogen treatment was at 0.86 atm and 65°C for 7 days. Sections of Ge/F-codoped fiber LA from the investigation of core/clad interfacial stress discussed in Section 3.3 of Interim Report No. 1 were used. Four samples were examined: (1) a pristine, as-drawn fiber, (2) a fiber irradiated to a dose of 20 krad without hydrogen treatment, (3) a hydrogen treated but unirradiated fiber, and (4) a hydrogen treated fiber irradiated to a dose of 17 krad. The hydrogen treatment was at 4 atm and 50°C for 10 days.

3.2.2 Photoluminescence Results

Regardless of history, both fiber compositions exhibit luminescence from at least two distinct centers. The first is an emission band at 650 nm which is generally believed to be associated with an absorption band at 630 nm. In the literature this center is reported to be caused by fiber drawing and irradiation [11,12,14]. It has been variously attributed to the nonbridging oxygen hole center (NBOHC) [13] or coexisting NBOHCs and nonparamagnetic electron traps [14]. The second center has a much broader emission band which peaks at $\approx$680 nm when excited by wavelengths $\lambda_{ex} < 530$ nm. This center was discussed in Interim Report No. 1 [2] and recently reported on by Wei *et al.* [10]. Although we have not measured its absorption spectrum, from the dependence of the emission intensity on λ_{ex} we surmise that it has at least one broad absorption band which peaks $\leq$470 nm. A luminescence band at 670-680 nm has also been reported for Ge-doped silica [15] and hydrogen treated Ge-doped and Ge/P-codoped fibers [16]. These bands are most likely due to the same center that we observe. The differences in shape, position, excitation spectrum, and photobleaching characteristics between the 650 nm and 680 nm luminescence bands unequivocally establishes that they are different centers. Since very few research groups have recognized that two distinct centers emit at almost the same wavelength in this spectral region, one must be cautious in interpreting the literature on the subject of the "1.9 eV (650 nm) center." The extreme breadth of the luminescence from the 680 nm center as well as the large Stokes shift (i.e., the difference in energy between the peaks of the absorption and emission bands) indicate that the electronic states of the responsible center are more strongly coupled to the lattice than those of the 650 nm center. This implies that the electronic transitions are accompanied by large structural relaxations of the complex. Although a third emission band at $\approx$720 nm is observed for Ge/F-codoped fiber, we find some evidence that this may be a perturbed 680 nm center rather than a distinct center.

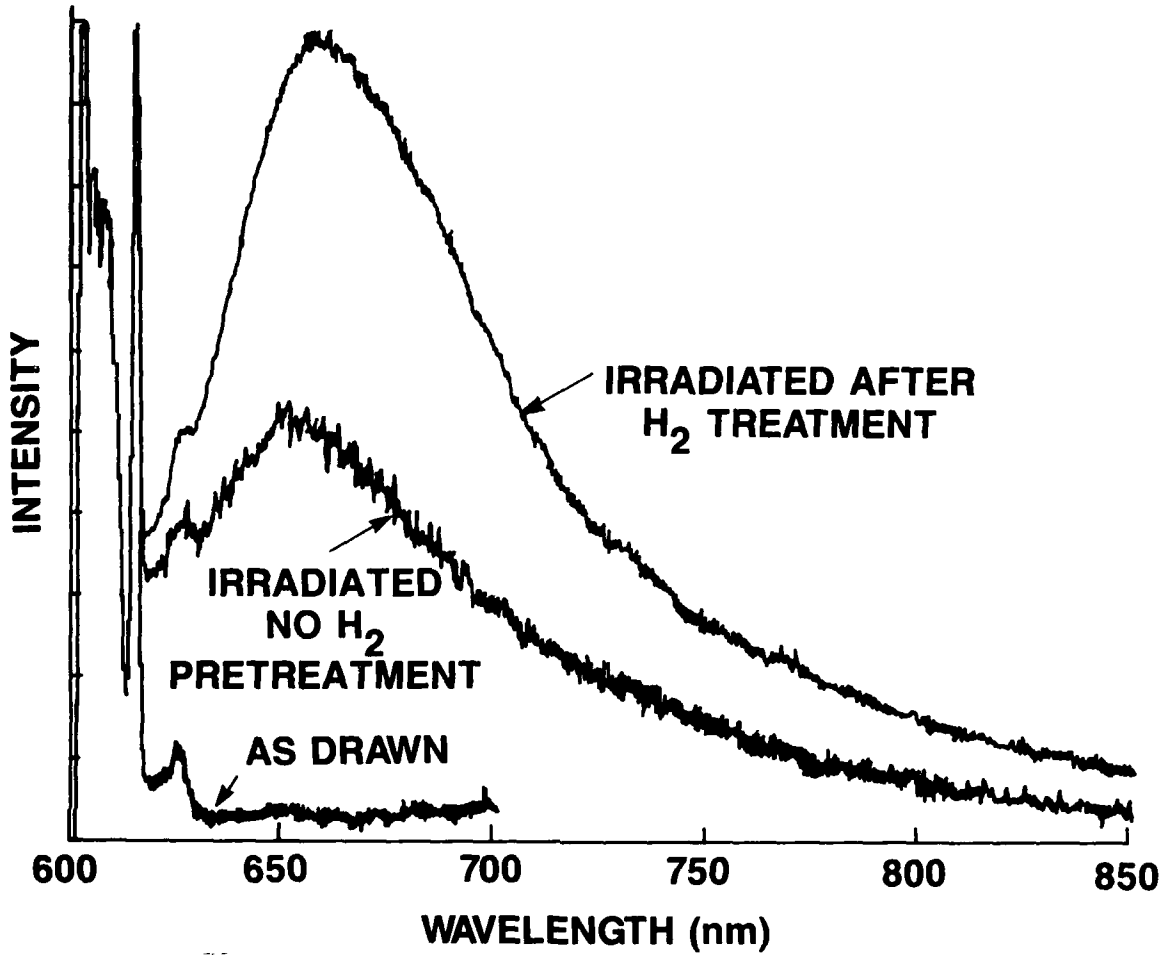

Figure 12: Comparison of luminescence spectrum prior to photobleaching for Ge/P-co-doped fibers, $\lambda_{ex} = 568$ nm. The sharp structure at left is Raman scattering which was used to provide an absolute comparison of intensities.

Figure 12 compares the luminescence band at 650 nm for the three Ge/P-codoped fibers before they were subjected to photobleaching. Luminescence is not detectable for the pristine fiber but is prominent for the irradiated fibers, being even more intense for the fiber that had been hydrogen treated before irradiation. Since the latter fiber also exhibited lower losses at wavelengths > 0.8 μm, this inverse relationship to radiation-induced loss implies that this defect does not significantly contribute to the induced long wavelength loss in these fibers. Moreover, it appears that hydrogen treatment can convert defects that will result in long wavelength losses when irradiated into the more benign defects responsible for this luminescent center. Figure 13 shows the corresponding comparison of the

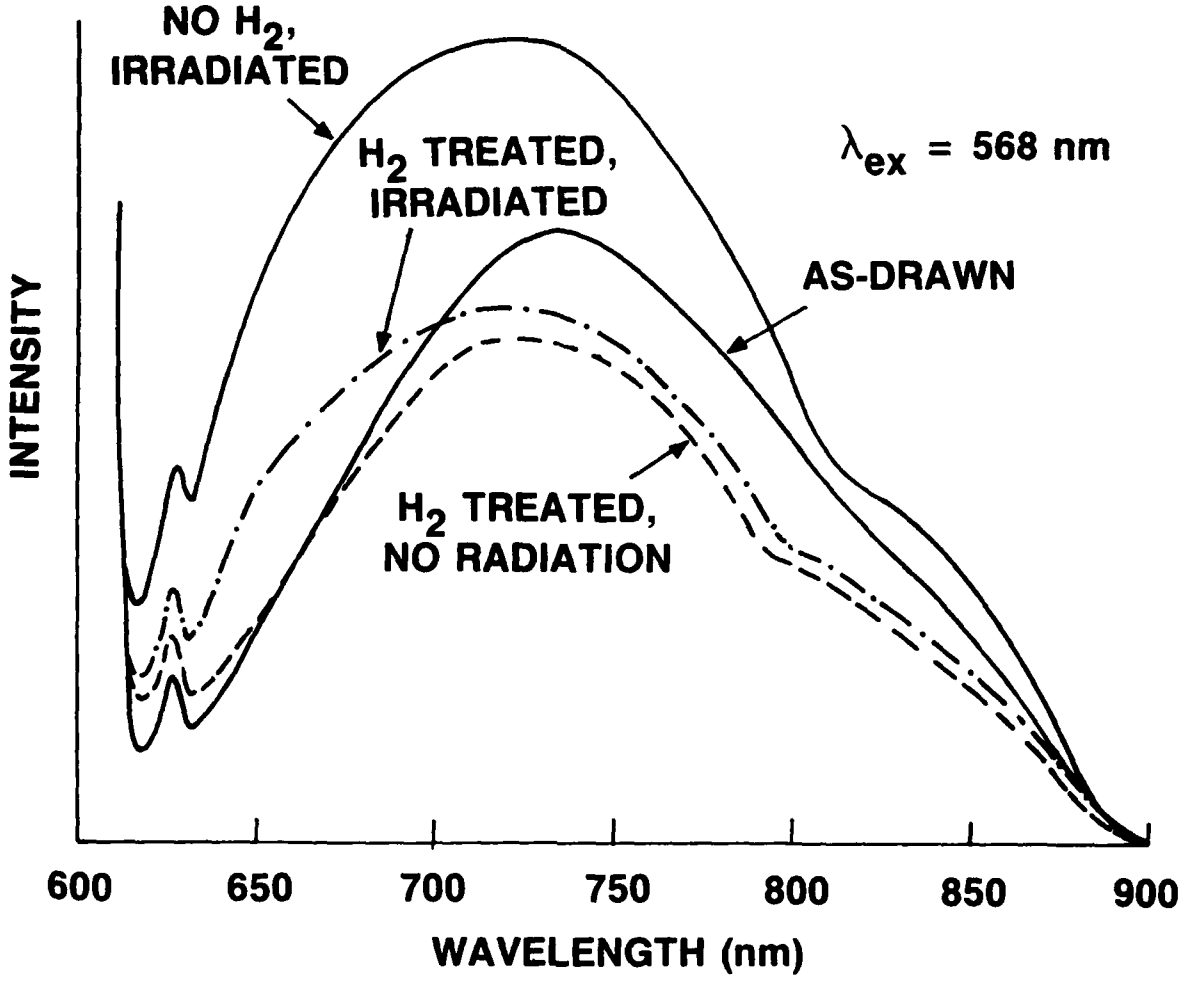

Figure 13: Comparison of luminescence spectrum prior to photobleaching for Ge/F-co-doped fibers, $\lambda_{ex} = 568$ nm. Sharp structure at left is Raman scattering which was used to provide an absolute comparison of intensities.

Ge/F-codoped fibers prior to photobleaching. The emission spectrum is now dominated by a very broad band peaking at ≈720 nm. Only for the irradiated fibers is there a slight shoulder at 650 nm indicating the presence of the 650 nm band. It is apparent from Figure 13 that irradiation increases the number of 720 nm centers, although the effect is less pronounced if the fiber has been pretreated with hydrogen. In addition, the increase is greater on the short wavelength side of the band. This is probably due to production of the 650 nm center, which, as for the Ge/P fiber, is greater if the fiber has been hydrogen treated. Note also that hydrogen treatment appears to suppress the formation of the 720 nm center, there being fewer of them even in the irradiated treated fiber than in the

as-drawn fiber. As with the 650 nm center, there is no apparent correlation between the 720 nm center and the induced long wavelength loss.

In general, changing λ_{ex} will excite a different set of color centers with a different emission spectrum. The 650 nm band observed for the Ge/P fibers is replaced by one peaking at $\approx$680 nm for excitation wavelengths $<$ 530 nm. This band is illustrated in Figure 14 which compares the emission for the three fibers with $\lambda_{ex} = 482$ nm. The fibers maintain the same hierarchy of intensities when excited at this wavelength, but the luminescence is considerably stronger with even the as-drawn fiber showing intense emission. The 680 nm band is also observed for the Ge/F fibers using the same excitation wavelengths. Figure 15 compares the emission of the four Ge/F fibers for $\lambda_{ex} = 476$ nm. The ordering of intensities is slightly different from that of the Ge/P fibers and from that excited by 568 nm in the same fibers. For the Ge/F fibers there is a rough correspondence between the concentration of the 680 nm center and fiber loss. Kashiwazaki *et al.* have reported a 680 nm emission band for Ge-doped silica VAD preforms and attributed it to a complex of Ge^{2+} and hydrogen [15]. However, Figure 15 contradicts their conclusion since it shows that, at least for the Ge/F fibers, the concentration of the responsible center is *decreased* by incorporating hydrogen into the glass.

The position and intensity of the 680 nm band is sensitive to the excitation wavelength for both fiber compositions. Over the range examined, 470 nm $< \lambda_{ex} <$ 530 nm, this band increases in intensity and shifts to shorter wavelength as λ_{ex} is moved to shorter wavelength. The intensity variation is an excitation efficiency effect resulting from the overlap of the excitation wavelength and the absorption band of the center. The dependence observed indicates that the peak of the absorption band lies $\leq$470 nm. This is in agreement with Kashiwazaki *et al.* who report 465 nm as the peak of the photoluminescence excitation spectrum for the 680 nm band they observe in Ge-doped silica preforms [15]. The band shifting is illustrated in Figure 16 for one of the Ge/F fibers. All the peaks have been normalized to full scale to facilitate spectral comparisons. The shift of the peak position is in the same direction as the change in λ_{ex}, indicating an extremely inhomogeneous distribution of sites for this center. This means that each particular center has a slightly different local environment which translates into a different absorption and emission spectrum. Changing λ_{ex} alters the set of centers that is most efficiently excited and the shift in the peak of the emission spectrum reflects this new distribution of excited centers. Although this inhomogeneous effect is observed for both fiber compositions, there is a difference at longer excitation wavelengths. As λ_{ex} is increased beyond $\approx$530 nm for

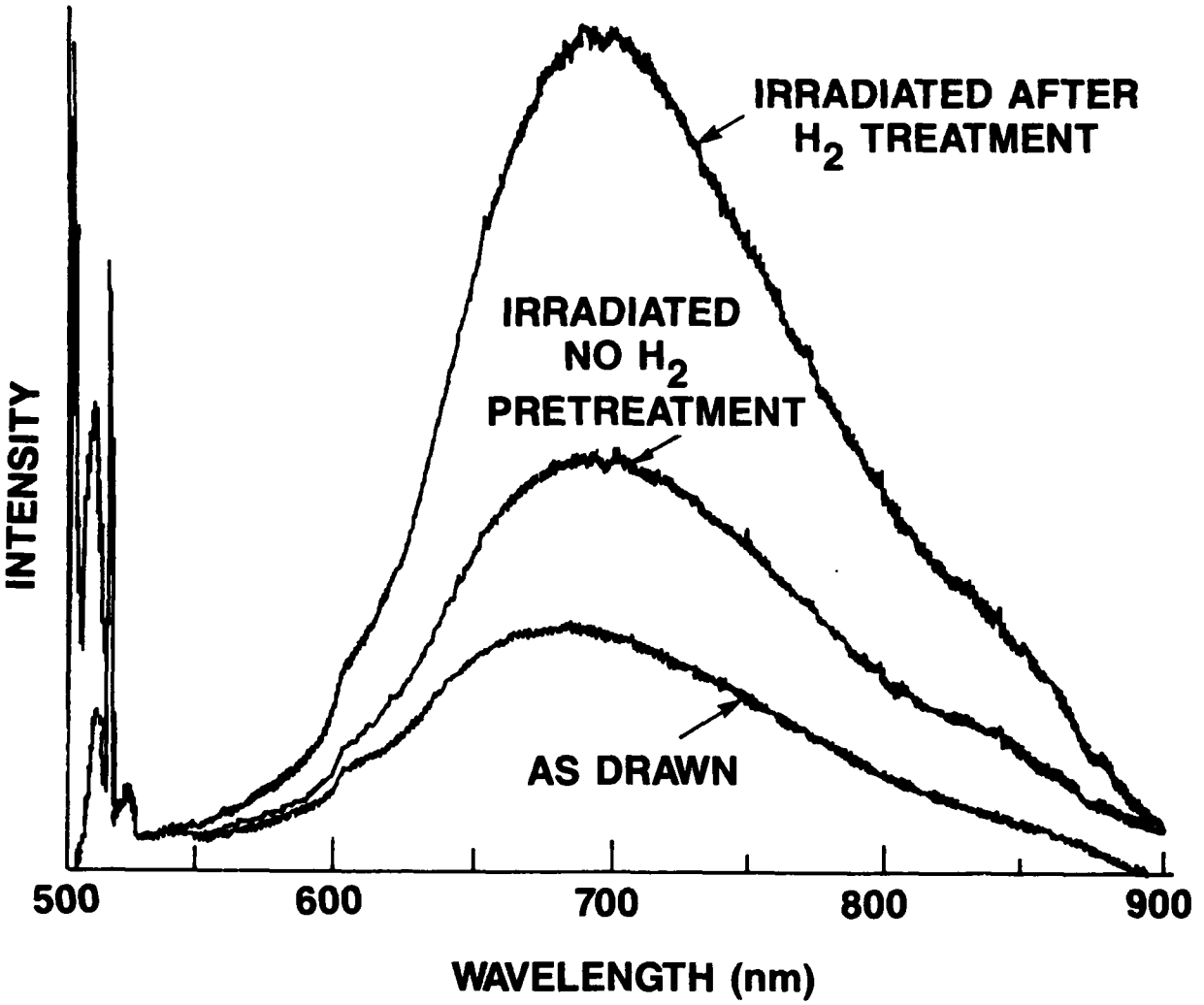

Figure 14: Comparison of luminescence spectrum prior to photobleaching for Ge/P-co-doped fibers, $\lambda_{ex} = 482$ nm. Sharp structure at left is Raman scattering which was used to provide an absolute comparison of intensities.

the Ge/F fibers, the 680 nm band continues to shift to longer wavelength and decrease in intensity until it becomes the 720 nm band observed for $\lambda_{ex} = 568$ nm. As λ_{ex} is increased beyond $\approx$530 nm for the Ge/P fibers, however, this band disappears and is replaced by the narrower 650 nm band. From these observations we believe that both the 720 nm and the 680 nm bands are due to the same general class of color center. The particular complex emitting at 720 nm, however, has been perturbed (possibly by fluorine) so that it absorbs and emits at longer wavelengths. This would be an extreme example of the inhomogeneous broadening mechanism outlined above.

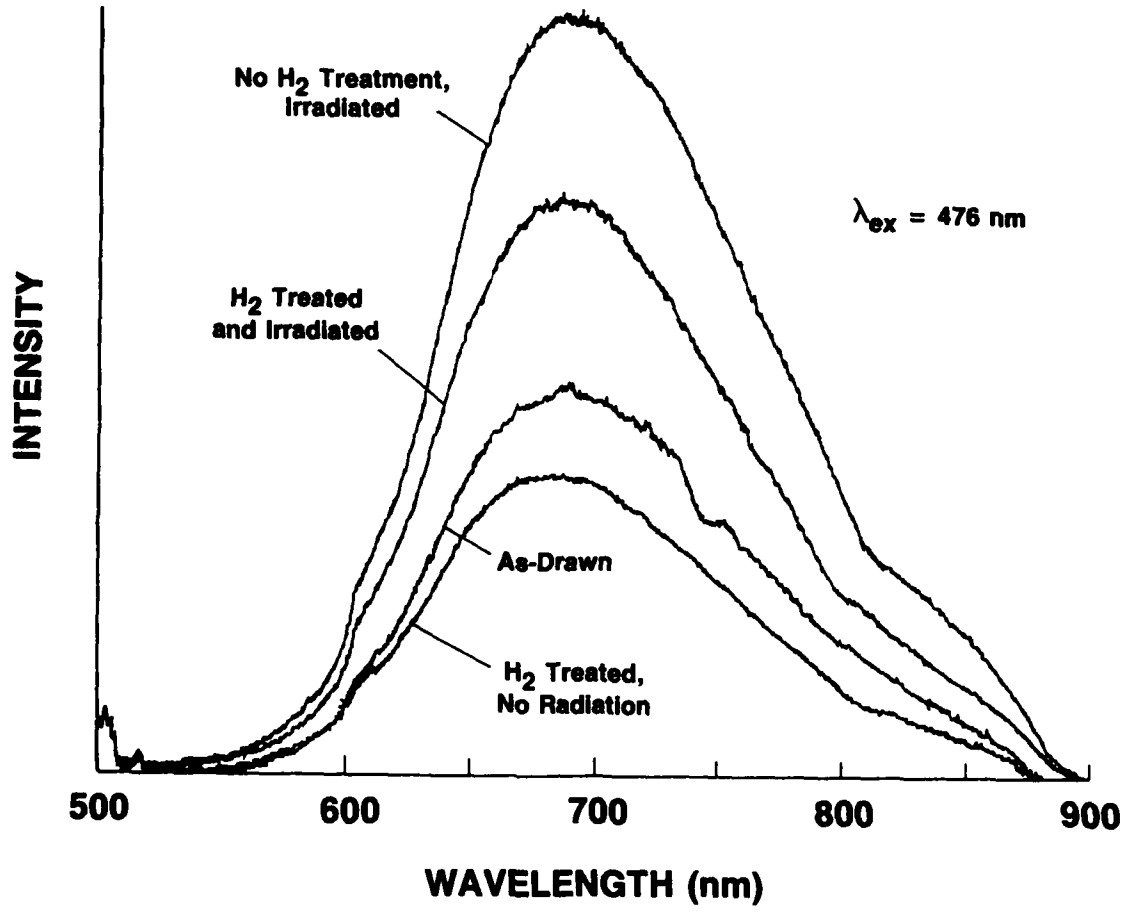

Figure 15: Comparison of luminescence spectrum prior to photobleaching for Ge/F-co-doped fibers, $\lambda_{ex} = 476$ nm. Weak features at ≈ 500 nm are Raman scattering which was used to provide an absolute comparison of intensities.

3.2.3 Photobleaching Results

Prolonged excitation at short wavelengths ($460 \text{ nm} < \lambda < 530$ nm) produced significant changes in color center populations for all fibers, including the as-drawn sample. This process was observed through changes in the photoluminescence spectra, but also manifested itself as photobleaching in the irradiated fibers. Although the fiber samples used for the luminescence investigation were too short to permit the loss spectrum to be remeasured, the photobleaching was readily observed through visual inspection of the highly darkened Ge/P fibers. This photoconversion process occurs through the photoionization

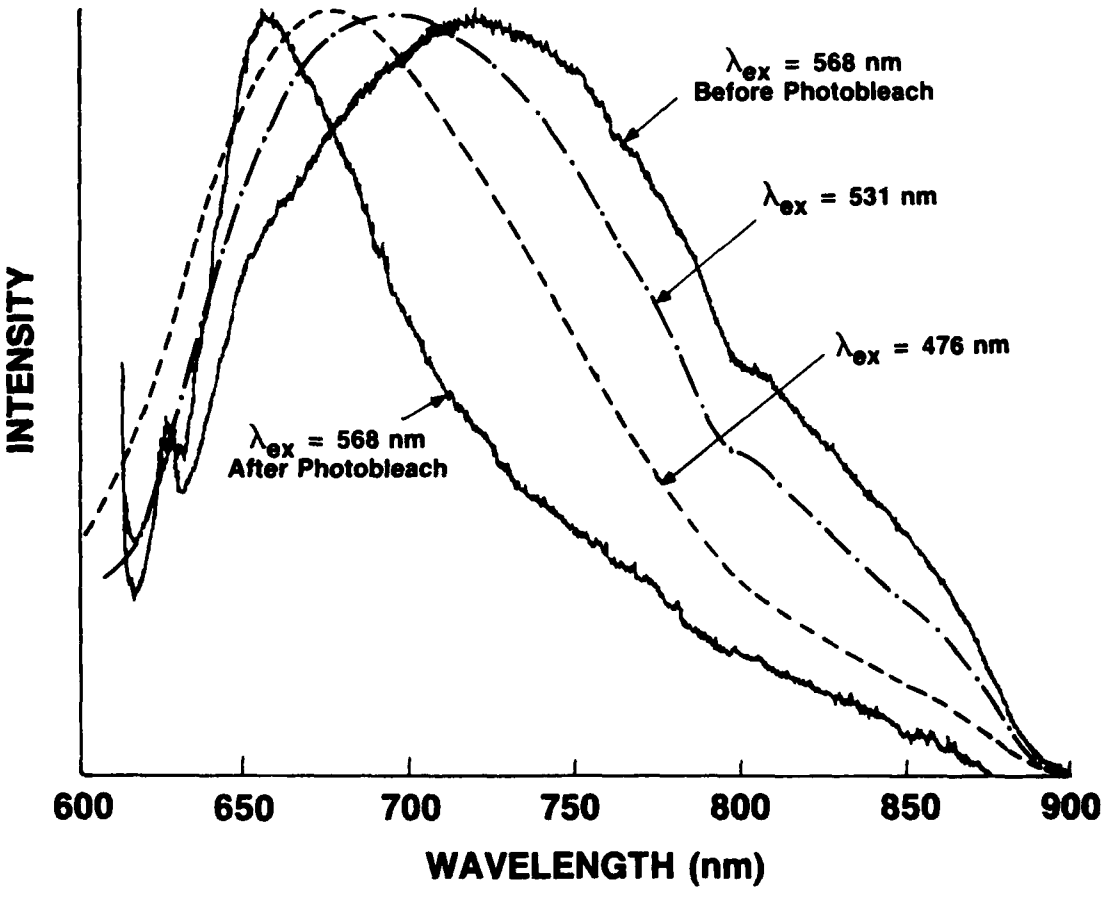

Figure 16: Shift in position of luminescence spectrum as a function of λ_{ex} for the Ge/F-co-doped fiber that was hydrogen treated prior to irradiation. All spectra were measured before photobleaching except for the indicated $\lambda_{ex} = 568$ nm spectrum which is provided for comparison purposes.

and retrapping of electrons and holes at existing defect centers. For all samples, including the as-drawn fiber, it was found that short wavelength exposure significantly reduced the intensity of the 680 nm band, indicating that the wavelengths effective at exciting the responsible center also destroy it. Noguchi *et al.* have reported that the defect band they observe at $\approx$660 nm for hydrogen treated fiber is also bleached by blue excitation [16]. This supports our view that this is the same color center. In contrast, Figure 17 illustrates the effect of photobleaching on the defect band at 650 nm for the Ge/P as-drawn fiber. Prior to the short wavelength exposure there had been no significant emission at 650 nm.

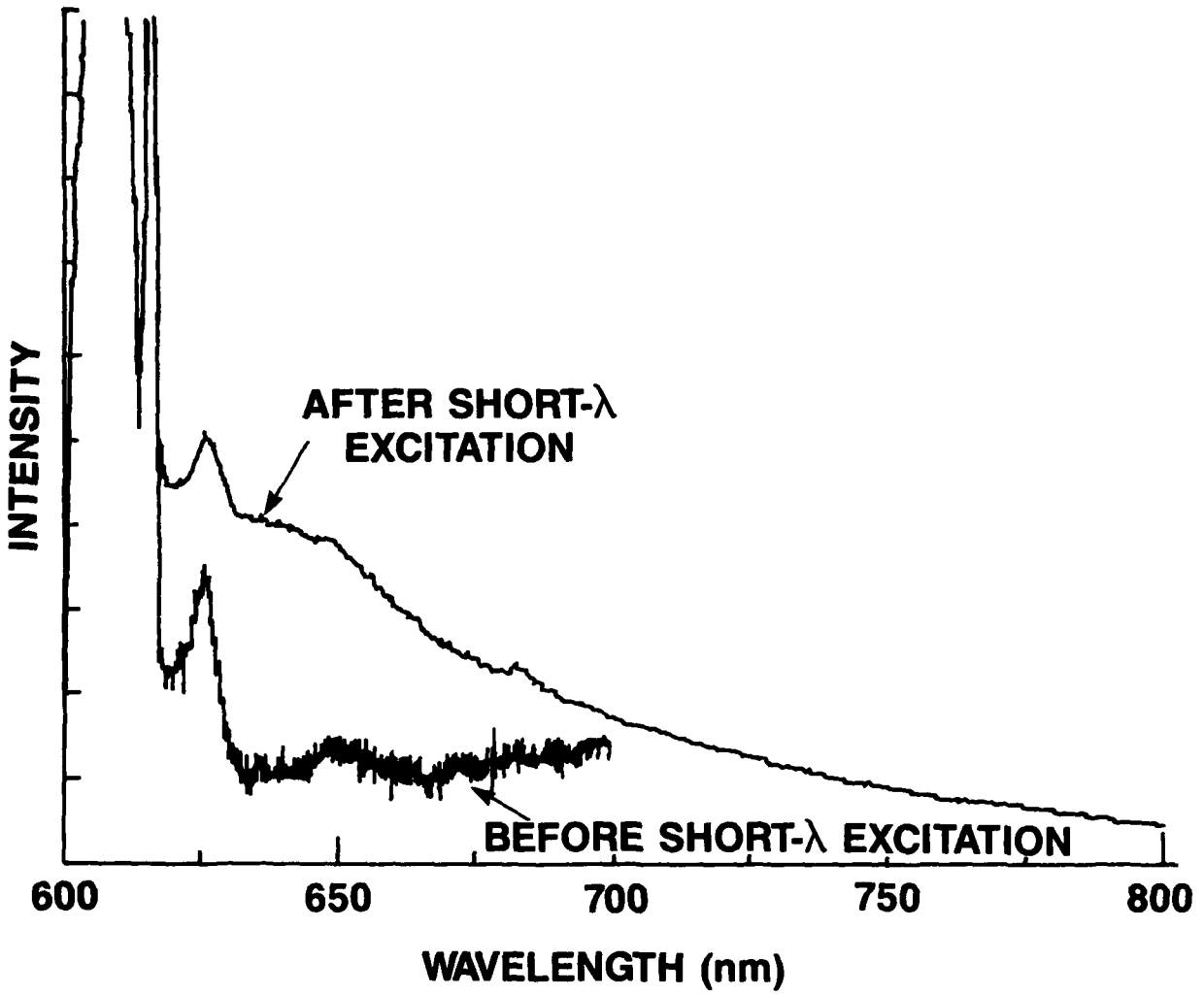

Figure 17: Comparison of luminescence spectrum before and after photobleaching for as-drawn Ge/P fiber, $\lambda_{ex} = 568$ nm. The sharp structure at left is Raman scattering which was used to provide an absolute comparison of intensities.

Afterwards the luminescence band has become noticeable although still much less intense than the Raman scattering. For all fibers examined this luminescence is considerably stronger following photobleaching, implying an increase in concentration of the center responsible for the 650 nm band although the fiber loss has been significantly reduced. A similar effect has been reported for Ge-doped fibers which were subjected to ultraviolet (350-370 nm) excitation [17]. Our observations establish that this photoconversion process is significant for blue light as well [9,10]. Figure 18 shows that the effect is even more pronounced for the Ge/P fiber that had been hydrogen treated prior to irradiation. Short wavelength exposure also increase the concentration of 650 nm center in the Ge/F fibers. In

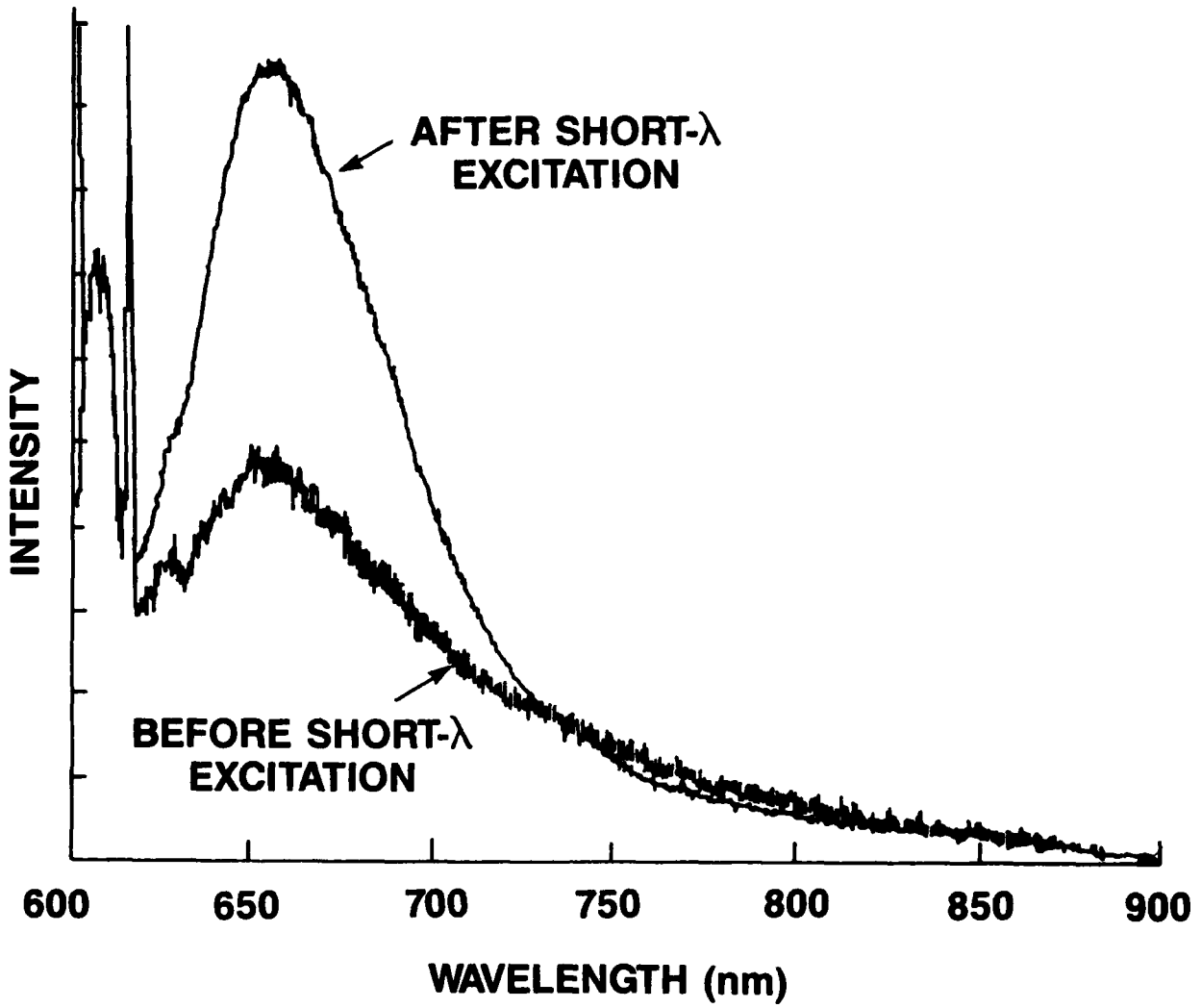

Figure 18: Comparison of luminescence spectrum before and after photobleaching for Ge/P fiber treated with hydrogen prior to irradiation, $\lambda_{ex} = 568$ nm. The sharp structure at left is Raman scattering which was used to provide an absolute comparison of intensities.

fact, only subsequent to photobleaching is this band clearly observed for these fibers. This effect is illustrated in Figure 19 for the fiber that was irradiated without hydrogen treatment. It is apparent that not only has the 650 nm band been increased by the short wavelength exposure, but the 720 nm band has been reduced. This effect can also be seen in the λ_{ex}-dependence of the luminescence illustrated in Figure 16. After photobleaching, the 720 nm emission band has been largely replaced by the 650 nm band for the Ge/F fiber. This is consistent with our interpretation of the 720 nm center as a perturbation of the center responsible for the 680 nm band, which is similarly photobleached. Figure 20 shows how the 650 nm band is, in turn, bleached by 568 nm excitation. This process, however, does not lead to the regeneration of the center responsible for the 680 nm band.

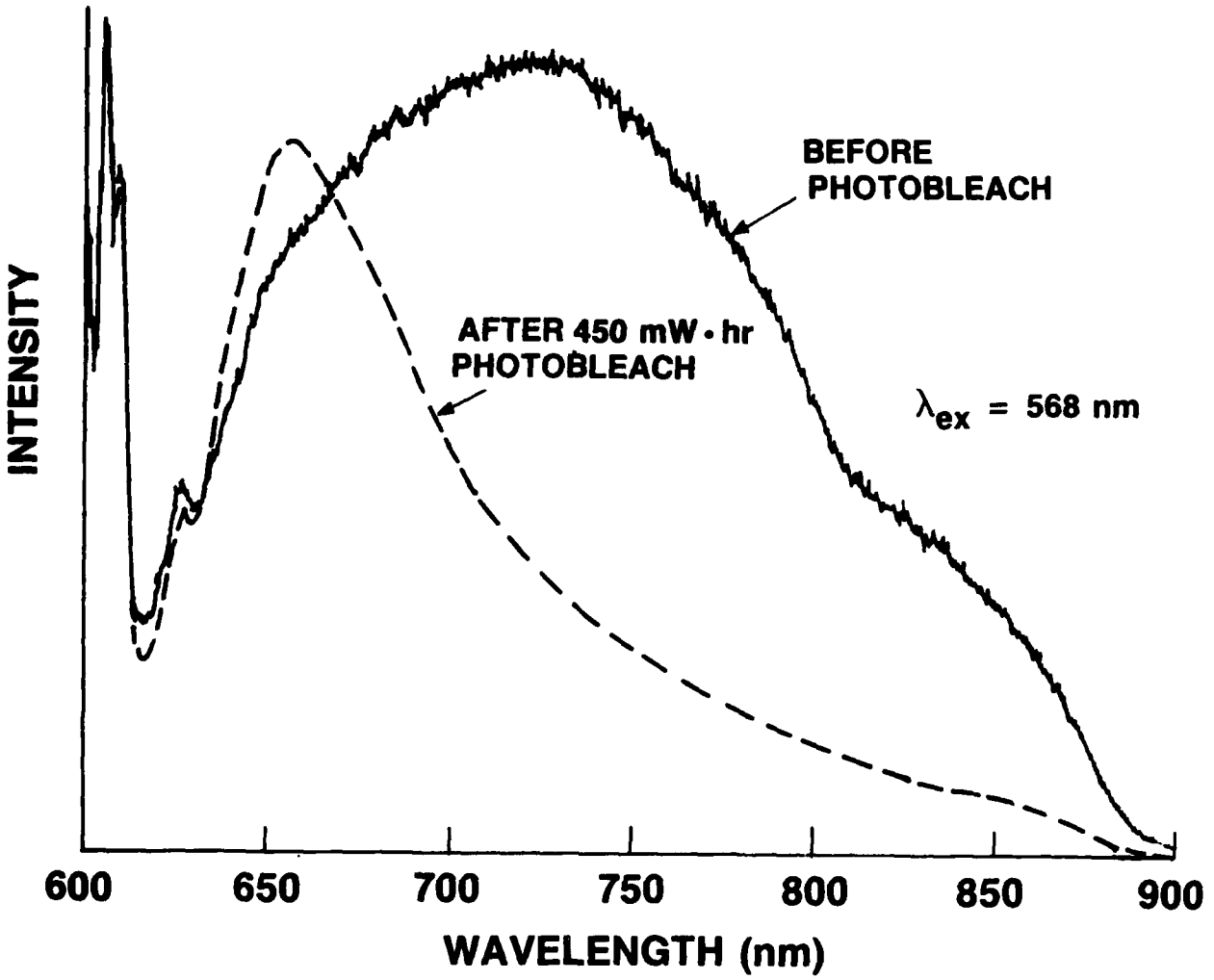

Figure 19: Comparison of luminescence spectrum before and after 450 mW•hr photobleach at 488 nm for $\lambda_{ex} = 568$ nm. The Ge/F fiber had been previously irradiated to 20 krad without hydrogen treatment. The sharp structure at left is Raman scattering which was used to provide an absolute comparison of intensities.

These results provide further evidence for our conclusion that there are at least two distinct defect centers absorbing in the visible spectral region. The 650 nm luminescence band has been reported in the literature; the nature of the center responsible is still a subject of controversy although most authors agree that it is associated with the NBOHC. The bleaching of this center is a new result arising from this investigation. Although we have not yet identified the defect band at 680 nm, our measurements contradict the assignment of Kashiwazaki *et al.* who propose that it is due to a complex of Ge^{2+} and hydrogen [15]. The evidence is persuasive that it is the same for both fiber compositions we investigated,

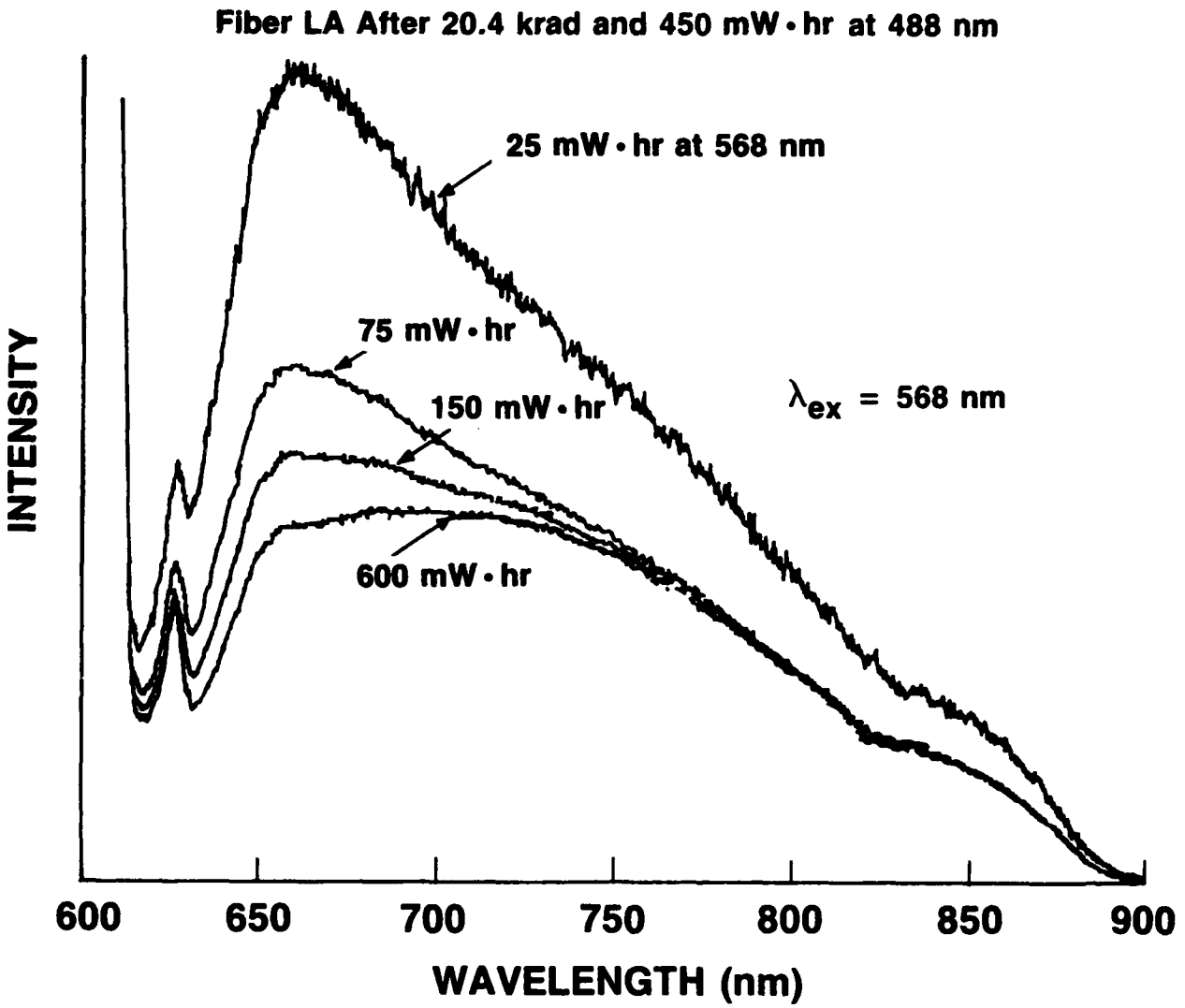

Figure 20: Photobleaching of 650 nm defect band by indicated amounts of 568 nm excitation, $\lambda_{ex} = 568$ nm. This is the same Ge/F fiber used for Figure 19. The sharp structure at left is Raman scattering which was used to provide an absolute comparison of intensities.

Ge-doped silica [15], and hydrogen-treated Ge-doped and Ge/P-codoped silica [16]. This center appears to be present at a greater concentration in the Ge/F fibers than in the Ge/P fibers. On the other hand, there seems to be a greater number of the 650 nm defects in the Ge/P fibers. The luminescence spectra of Ge/F-codoped fibers for $\lambda_{ex} = 568$ nm differ from from those of Ge/P-codoped fibers in showing the presence of the 720 nm centers and fewer of the 650 nm defects. The former center we tentatively attribute to perturbations of the 680 nm defect that emit and absorb at longer wavelengths than the majority of the centers. It is possible that fluorine ions are responsible for the perturbation.

4. RECOMBINATION CENTER APPROACH

The basis of the recombination center approach is to provide trapping centers for the electrons and holes generated by the ionizing radiation. These centers need to capture both an electron and a hole which then recombine, freeing the center to repeat the scavenging process. If these centers can compete successfully with deleterious precursor defects for the electrons and holes, they may suppress color center formation. The standard procedure is to dope the preform with one of the multivalent ions (e.g., arsenic, antimony, cerium) used to reduce solarization of glass.

To investigate the role of recombination centers in reducing the radiation hardness of optical fiber, we developed special deposition techniques for incorporating cerium into optical fibers using an MCVD preform fabrication system. The relatively volatile Ce organic complex $Ce(fod)_4$ was selected as the starting material. The abbreviation fod stands for tetrakis 6,6,7,7,8,8,8-heptafluoro-2,3-dimethyl-3,5-octanedione. This compound had previously been used for cerium doping using an outside deposition process [18]. In our implementation, its vapor was transported directly downstream into the reactant flow and subsequently reacted to form the cerium dopant in the hot zone. Several Ge/Ce-codoped fibers with different Ce concentrations were fabricated using this technique.

The first step was the synthesis of $Ce(fod)_4$ in our laboratories. The complex was then dissolved in acetone and placed in a special enlarged section of the substrate tube located upstream from the primary deposition zone. The solvent was completely removed by purging with dry nitrogen overnight. During the core deposition passes, the reservoir was heated to $\approx$200°C by heat guns to produce $Ce(fod)_4$ vapor, which was transported to the hot zone by oxygen with which it then reacted to form soot for the Ge/Ce-codoped core.

The preform core was observed to be colorless. However, when it was excited by a uv source, the core fluoresced a blue/green color, indicating the presence of Ce^{3+}. Absorption measurements on preform slices revealed broad absorption bands at 320 nm and 240 nm characteristic of Ce^{3+} and Ce^{4+}, respectively [19]. It should be noted that the assignment of these absorption bands to the corresponding Ce valence states was reversed by the authors of Ref. 18. Spark source mass spectrographic analysis indicated

the Ce concentrations ranged from 100 to 300 ppm by weight, depending upon the flow rates of the reactants and the temperature of the $Ce(fod)_4$ reservoir.

The loss spectrum of the fiber prior to irradiation showed a hydroxyl level of 1 ppm, which was much higher than that of our standard fibers without Ce. Both hydroxyl and other impurities may be related to the decomposition of $Ce(fod)_4$ at high temperatures, particularly since the hydrogen in this compound has not been completely replaced by fluorine. Attempts to dehydrate the doped preform before sintering failed because of the instability of $Ce(fod)_4$ in Cl. The contamination caused by the decomposition as well as the reaction with Cl has so far prevented the fabrication of low loss fibers.

Figure 21 illustrates the loss spectrum of a Ge/Ce-codoped fiber before and after an 18 krad irradiation. This fiber showed relatively poor radiation resistance. However, it is not known if this is because Ce doping itself introduces additional defects or whether it is due to the hydroxyl and other impurities introduced by the doping process. Because the recombination center approach is fraught with such difficulties and uncertainties, we decided to abandon it after the Exploratory Phase and concentrate on the technical approaches that yielded better results.

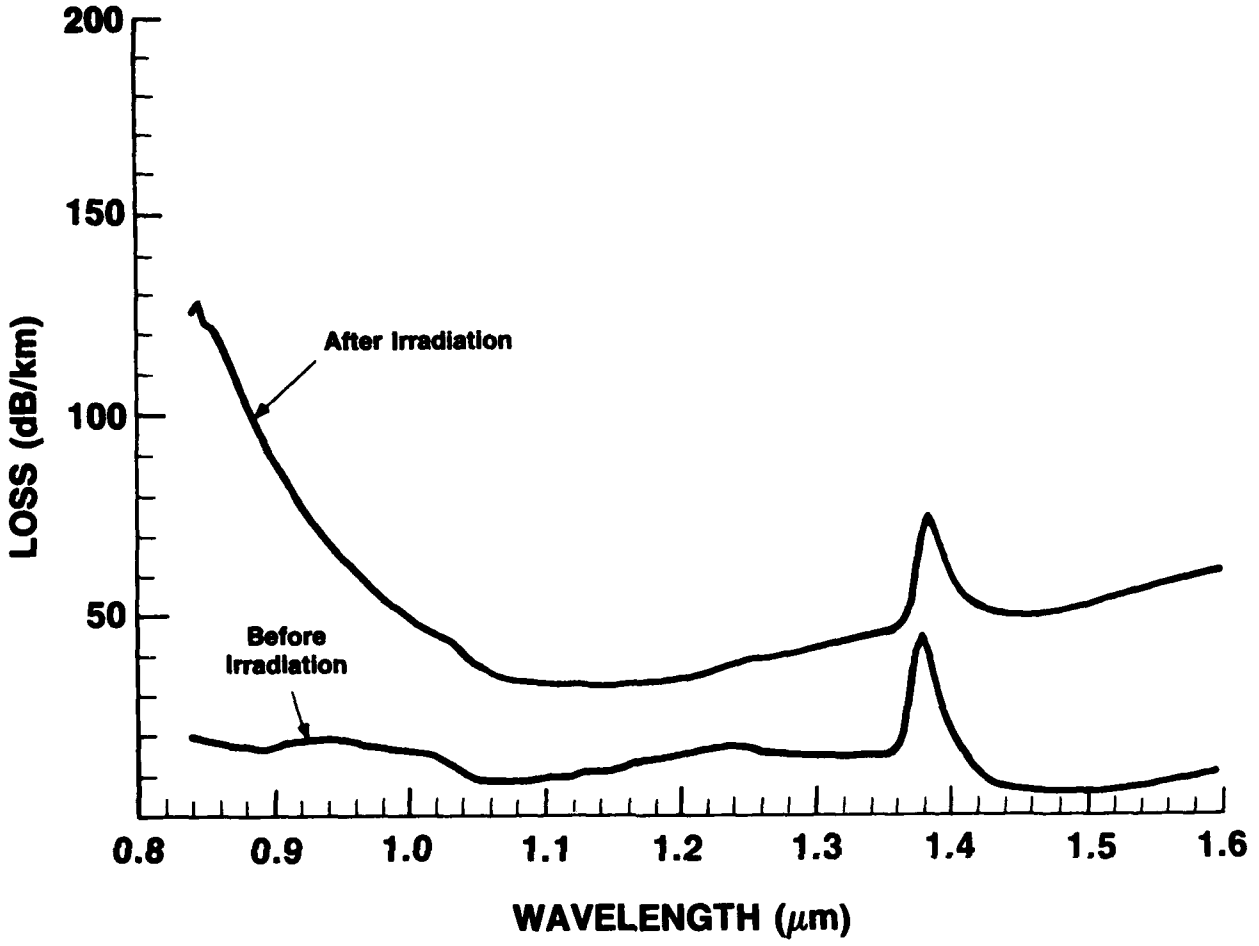

Figure 21: Comparison of loss spectrum before and after irradiation for Ge/Ce-codoped fiber.

5. REFERENCES

[1] E.J. Friebele, K.J. Long, C.G. Askins, M.E. Gingerich, M.J. Marrone, and D.L. Griscom, SPIE ***541***, 70 (1985).

[2] W.J. Miniscalco, T. Wei, and P.I.K. Onorato, "Radiation Hardened Silica-Based Optical Fiber," Interim Report RADC-TR-86-181, Oct. 1986.

[3] H. Hanafusa, Y. Hibino, H. Itoh, and F. Yamamoto, Electron. Lett. ***23***, 10 (1987).

[4] M. Ogai, A. Iino, and K. Matsubara, Tech. Digest OFC/IOOC '87, postdeadline paper No. PDP3 (1987).

[5] T. Gozen, H. Tanaka, A. Utsumi, T. Maeda, and S. Okamoto, *Proc. 1984 Conf. on Elect. Insul. and Dielect. Phenom.*, p. 65 (IEEE, Piscataway, NJ, 1984).

[6] S. Shibata and M. Nakahara, J. Lightwave Technol. ***LT-3***, 860 (1985).

[7] R.B. Greegor, F.W. Lytle, J. Kortright, A. Fischer-Colbrie, J. Non-Cryst. Sol. ***89***, 311 (1987).

[8] S.H. Garofalini, J. Non-Cryst. Sol. ***63***, 337 (1984).

[9] T. Wei, M.P. Singh, W.J. Miniscalco, and J.A. Wall, SPIE ***721***, 32 (1987); this article is included as Appendix A.

[10] T. Wei, M.P. Singh, W.J. Miniscalco, and J.A. Wall, Mat. Res. Soc. Symp. Proc. ***88***, 207 (1987); this article is included as Appendix B.

[11] M.J. Marrone, Appl. Phys. Lett. ***38***, 115 (1981).

[12] W. Carvalho, P. Dumas, J. Corset, and V. Neumann, in *Proceedings of Optical Fibers in Adverse Environments*, SPIE Vol. ***404***, p. 76 (1983).

[13] L.N. Skuja, A.R. Silin, and A.G. Boganov, J. Non-Cryst. Solids **63**, 431 (1984).

[14] E.J. Friebele, D.L. Griscom, and M.J. Marrone, J. Non-Cryst. Solids ***71***, 133 (1985).

[15] A. Kashiwazaki, K. Muta, M. Kohketsu, and H. Kawazoe, Mat. Res. Soc. Symp. Proc. ***88***, 217 (1987).

[16] K. Noguchi, N. Uesugi, N. Shibata, K. Ishihara, and Y. Negishi, Electron. Lett.***21***, 438 (1985).

[17] K. Noguchi, N. Uesugi, and K. Suzuki, Electron. Lett. ***22***, 619 (1986).

[18] D.A. Thompson, P.L. Bocko, and J.R. Gannon, SPIE ***506***, 170 (1984).

[19] J.S. Stroud, J. Chem. Phys. ***35***, 844 (1961).

APPENDIX A

Reprinted from SPIE Vol. 721 – Fiber Optics in Adverse Environments III

Effect of Hydrogen Treatment on Radiation Hardness of Optical Fiber

T. Wei, M.P. Singh, and W.J. Miniscalco

GTE Laboratories Incorportated
40 Sylvan Road
Waltham, MA 02254

J.A. Wall

Rome Air Development Center:ESR
Hanscom AFB, MA 01731

Reprinted from SPIE Vol 721 —Fiber Optics in Adverse Environments III
1987 by the Society of Photo-Optical Instrumentation Engineers Box 10 Bellingham WA 98227 0010 USA

Effect of hydrogen treatment on radiation hardness of optical fibers

T. Wei, M.P. Singh, and W.J. Miniscalco
GTE Laboratories Inc., 40 Sylvan Road, Waltham, Massachusetts 02254

and

J.A. Wall
Rome Air Development Center: ESR
Hanscom AFB, Massachusetts 01731

Abstract

We have treated optical fibers in different hydrogen environments to examine the effect of hydrogen treatment on radiation hardness of optical fibers. Both radiation-induced loss and hydrogen-induced loss are related to defect center formation in optical fibers. We have investigated the effects of treatment conditions on defects produced by drawing and γ-irradiation using the techniques of spectral attenuation, Raman scattering, and photoluminescence.

Using Ge/P-codoped multimode optical fibers, we observed considerable reduction in the radiation-induced absorption at long wavelengths ($\lambda > 1$ μm) for hydrogen-treated fibers. Post-treatment of irradiated fibers by hydrogen can also reduce existing radiation-induced absorption significantly and increase the hardness of the fibers under subsequent irradiation. For Ge/F-codoped multimode fibers, hydrogen treatment has also shown its effectiveness in enhancing radiation hardness. The pretreated fibers show $\cong$15% improvement at 850 nm in radiation resistance over untreated fibers. Varying the hydrogen treatment and irradiation history of the fiber had little effect upon the Raman spectrum. However, significant trends were found in the behavior of the photoluminescence. Emission bands in the 600–900 nm spectral region have been found to have intensities which depend upon fiber history.

We attribute the improvement in radiation resistance to the passivation of precursors or defects in the optical fiber. Treatment with hydrogen converts certain types of defects into types which do not form deleterious color centers after irradiation. This defect-conversion interpretation is supported by the photoluminescence measurements which reveal variations in color center concentrations with hydrogen treatment, γ-irradiation, and optical excitation.

Introduction

Radiation-induced loss in glass is due to color centers which form when existing defects trap the electrons and holes generated by ionizing radiation. One method to prevent defects in as-drawn fiber from capturing carriers and forming color centers is to transform them into benign defects which do not absorb in the spectral region of interest. This approach has already been exploited in reducing radiation damage in bulk vitreous silica through the use of hydrothermal treatment.[1] The effect of water is to transform an E′ defect and a nonbridging oxygen into two neutral silanol groups. Similar studies indicated that fibers with high hydroxyl content were less prone to damage at short wavelengths, although excessive hydroxyl absorption was observed at long wavelengths.[2] Recently there have been many studies on increases of optical attenuation in optical fibers due to hydrogen permeation.[3] This loss increase phenomenon is associated with the diffusion of hydrogen to the fiber core and subsequent chemical reactions with structural defects in the glass to form OH species and new defect centers. To test the applicability of hydrogen treatment in defect passivation, we have compared the radiation resistance of a treated fiber with that of an untreated length of the same fiber. In addition to spectral attenuation measurements, Raman scattering and photoluminescence investigations have been undertaken to identify specific centers. Although Raman scattering was found to be insensitive to the centers of interest, photoluminescence has proven to be an effective tool. Using the latter technique, significant differences were found among fibers subjected to different treatments.

Hydrogen treatment

Ge/P-codoped fibers

In the first experiment we treated a 250-m-long section from a Ge/P-codoped, graded-index optical fiber. This piece was placed in an atmosphere with a hydrogen partial pressure of 0.06 atm at 70°C for 7 days. After the treatment, dissolved hydrogen was evacuated from the fiber. The hydroxyl concentration increased from 73 ppb to 115 ppb.

Portions of the hydrogen treated fiber and an untreated control fiber were irradiated using the ^{60}Co source at RADC to a total dose of ≅5 krad. Figure 1 shows the loss spectra from 800–1600 nm for the treated and untreated fibers after irradiation. The high loss at shorter wavelengths is expected for a phosphorus-doped optical fiber.[4] These measurements reveal a clear difference between the treated and untreated fibers which increases with increasing wavelength (Figure 1). The attenuation (dB/km) is ≅20% lower for the hydrogen-treated fiber at 1600 nm.

In the second experiment we treated fibers in an atmosphere with a hydrogen partial pressure of 0.86 atm at 65 °C for 7 days to observe effects of higher hydrogen partial pressure and hydrogen post-treatment on radiation-induced losses. Three samples were selected for the hydrogen treatment: both of the irradiated fibers from the first experiment and a piece of the as-drawn fiber. Figure 2 shows the loss spectra of the irradiated fibers after the hydrogen post-treatment. The data reveal a dramatic recovery in attenuation to 10–25 dB/km at 1100 nm, and 20–30 dB/km at 850 nm. All treated fibers and a control sample were subjected to ≅5 krad γ irradiation. Figure 3 compares the loss spectra after irradiation with and without the hydrogen treatment. We observe on the order of 50 dB/km less induced attenuation at long wavelengths ($\lambda > 1$ μm) for a hydrogen-treated fiber. This is significantly better than results from the first experiment and is attributed to the use of a higher hydrogen partial pressure. We also observed improvement in radiation hardness as a result of postirradiation hydrogen treatment. Post-treatment of irradiated fibers by hydrogen can reduce existing radiation-induced absorption (see Figure 2) and increase the hardness of fibers under subsequent irradiation. Figure 4 shows the loss spectra after a second irradiation for post-treated fibers. Note that there is little difference between two post-treated fibers and the overall loss is lower than that shown in Figure 3. Short sections of fibers from this study were subjected to Raman scattering and photoluminescence investigations.

Ge/F-codoped fibers

To evaluate the effect of hydrogen treatment for fibers with greater radiation resistance, we chose two Ge/F-codoped optical fibers which had been designed for an investigation of core/clad interfacial stress. In this investigation, the fiber with high core/clad interfacial stress was designated HA while that with low stress was designated LA. Both fibers have similarly low radiation sensitivities, as illustrated in Figure 5 for fiber LA. Two 250-m sections of fibers HA and LA were treated in 4 atm hydrogen at 50 °C for 10 days. After hydrogen pretreatment, fiber HA showed an increase of 18 ppb in hydroxyl concentration, while fiber LA showed very little change in hydroxyl concentration. The different behavior in reaction with hydrogen between these two fibers is believed to be due to the stress difference. Both treated fibers were irradiated at RADC to a total dose of ≅18 krad. Figures 6 and 7 compare loss spectra before and after irradiation for hydrogen-treated fibers HA and LA, respectively. Table 1 summarizes the induced loss results for fibers with and without hydrogen treatment. These measurements demonstrate that hydrogen treatment is effective in enhancing radiation hardness even for fibers with low radiation sensitivity. The treated fibers show ≅15% improvement at 850 nm in radiation hardness over untreated fibers.

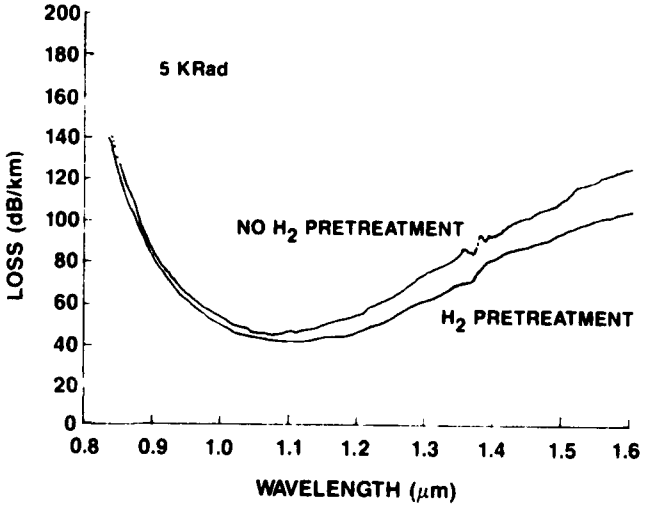

Figure 1. Loss spectra of fibers with and without hydrogen pretreatment (0.06 atm, 70 °C, 7 days) after 5 krad dose.

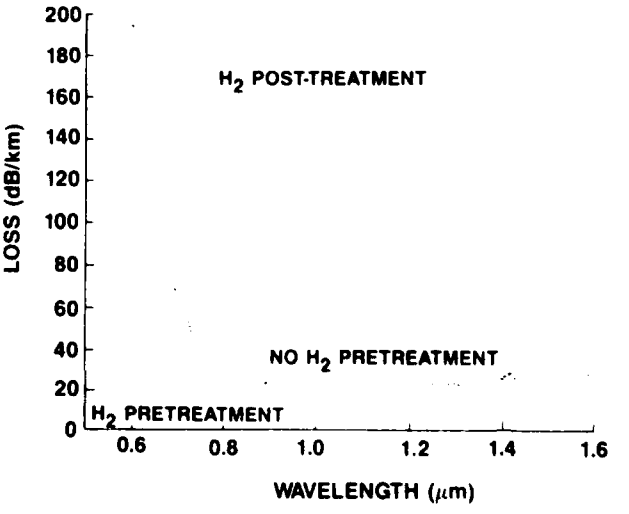

Figure 2. Loss spectra of fibers re-treated (0.86 atm, 65 °C, 7 days) after irradiation. Lower curve: with hydrogen pretreatment (0.06 atm, 70 °C, 7 days). Upper curve: without hydrogen pretreatment.

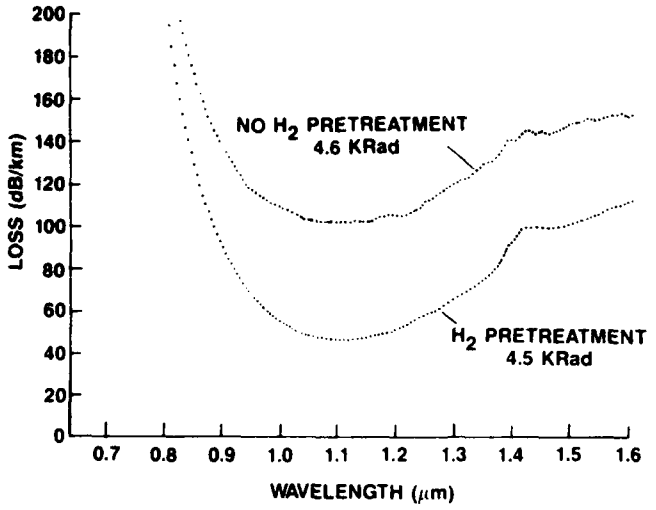

Figure 3. Loss spectra after 4.6 krad dose for fibers with and without hydrogen pretreatment (0.86 atm, 65°C, 7 days).

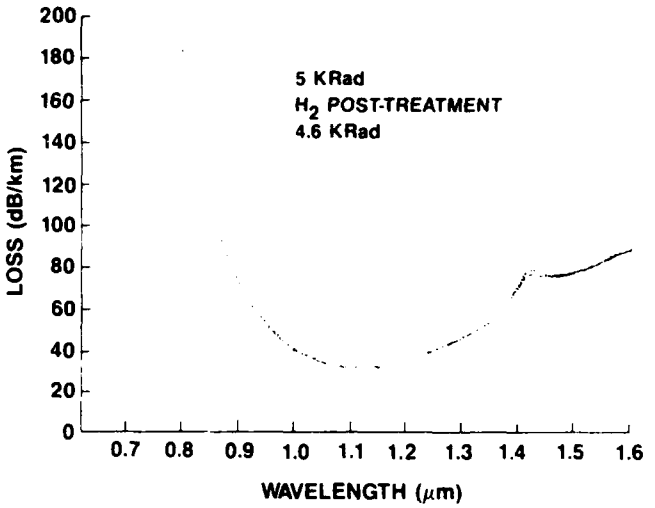

Figure 4. Loss spectra after a second 4.6 krad dose for fibers treated with hydrogen (0.86 atm, 65°C, 7 days) following first irradiation. The upper curve is the fiber which was treated prior to the first irradiation (0.06 atm, 70°C, 7 days).

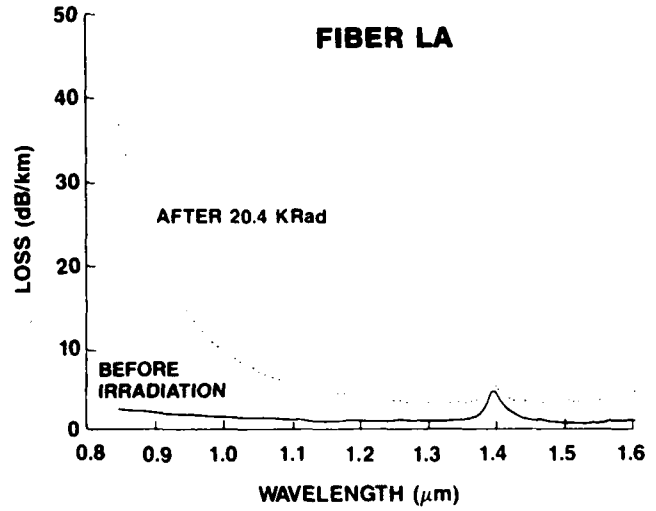

Figure 5. Loss spectra of low stress fiber LA before and after irradiation.

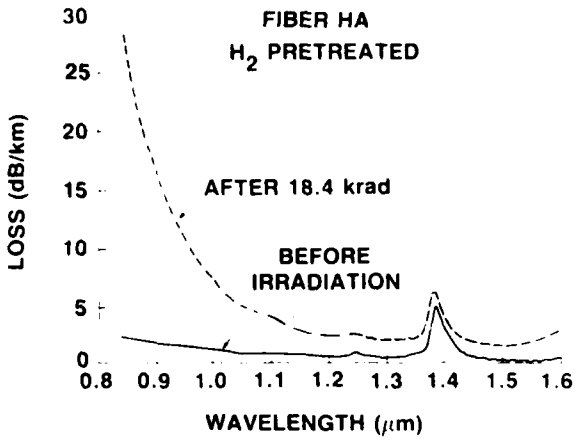

Figure 6. Loss spectra of hydrogen pretreated high stress fiber HA before and after irradiation.

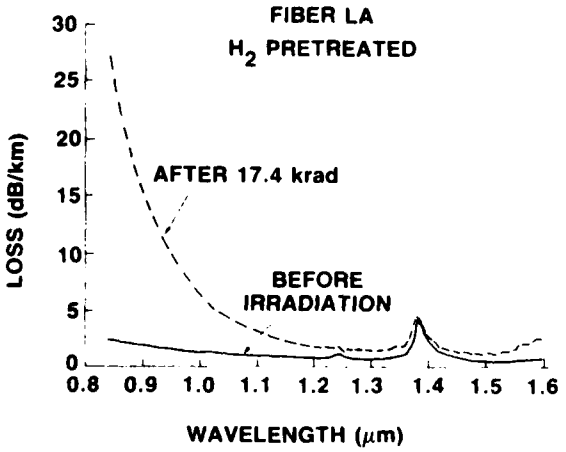

Figure 7. Loss spectra of hydrogen pretreated low stress fiber LA before and after irradiation

Table 1
Radiation-induced loss for hydrogen treated and untreated fibers

Fiber Designation	Hydrogen Treatment	Radiation-Induced Loss (dB/km/krad)	
		850 nm	1300 nm
HA	No	1.55	0.03
HA	Yes	1.28	0.08
LA	No	1.51	0.11
LA	Yes	1.29	0.04

Photoluminescence and Raman scattering

The radiation-induced loss measurements, which are the primary characterization tool used in this program, are generally not selective enough to identify the specific centers which are responsible for the absorption. In order to obtain a more selective technique for this purpose, we have explored the use of Raman scattering and photoluminescence to identify specific color centers and precursor defects in fibers and correlate their concentrations with preform composition and fiber processing.

Three of the phosphorus-doped fibers discussed above were investigated. These were a pristine as-drawn fiber, a fiber which was irradiated without pretreatment, and a fiber which was hydrogen treated and then irradiated. Raman scattering was performed on these fibers using laser excitation at wavelengths ranging from 482–676 nm. However, it was found to be relatively insensitive to the defects of interest, and no variations could be found among the fibers or as a function of wavelength for a given fiber. Photoluminescence was found to be a very sensitive probe of defect centers, and significant differences among the fibers were detected. Figure 8 compares the luminescence band at 650 nm for the three fibers before they were subjected to short wavelength ($\lambda < 530$ nm) excitation. This emission band and an associated absorption band near 630 nm have been reported on by several authors who attribute it to drawing- and/or radiation-induced centers.[5] To make an absolute comparison of intensities, the emission spectra were scaled by equalizing the intensities of the Raman scattering for the different fibers. Luminescence is not detectable for the pristine fiber but is prominent for the irradiated fibers, being even more intense for the fiber which had been hydrogen treated before irradiation. Since the latter fiber also exhibited lower losses at wavelengths >1 μm (lower curve in Figure 3), this inverse relationship to radiation-induced loss implies that this center is not responsible for the induced long wavelength loss in these fibers. Moreover, it appears that hydrogen treatment prior to irradiation can convert defects which will result in long wavelength losses into the more benign defects which are transformed into this luminescent center when irradiated.

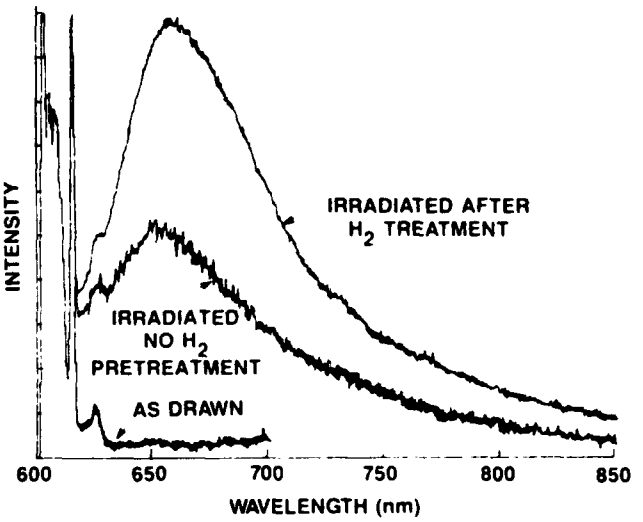

Figure 8. Comparison of luminescence intensity prior to excitation at 482 nm for fibers subjected to different treatments. The excitation wavelength was 568 nm. The sharp structure at left is Raman scattering which was used to scale the intensities for the different fibers.

Prolonged excitation at short wavelengths ($\lambda < 530$ nm) produced significant photobleaching in the irradiated fibers, which was observed through visual inspection. This occurs through photoconversion of centers, which is also observed through changes in photoluminescence intensity for all fibers, including the unirradiated fiber. Figure 9 illustrates this phenomenon for the latter. Prior to short wavelength exposure there had been no significant emission at 650 nm when excited at 568 nm. Afterwards the luminescence band has become noticeable although still much less intense than the Raman scattering. Figure 10 shows the same effect for the fiber which had been hydrogen treated prior to irradiation. The luminescence is considerably stronger, implying an increase in concentration of the center, although the fiber loss has been significantly reduced by photobleaching.

Photoconversion of defects is a well-known phenomenon in insulators, and its manifestation as photobleaching has been extensively studied in fibers. This investigation has provided additional evidence that radiation-induced loss can be reduced by defect conversion (passivation) before, as well as after, irradiation. The center responsible for the 650-nm luminescence band is an example of a relatively benign defect which can be formed by hydrogen treatment from more deleterious defects.

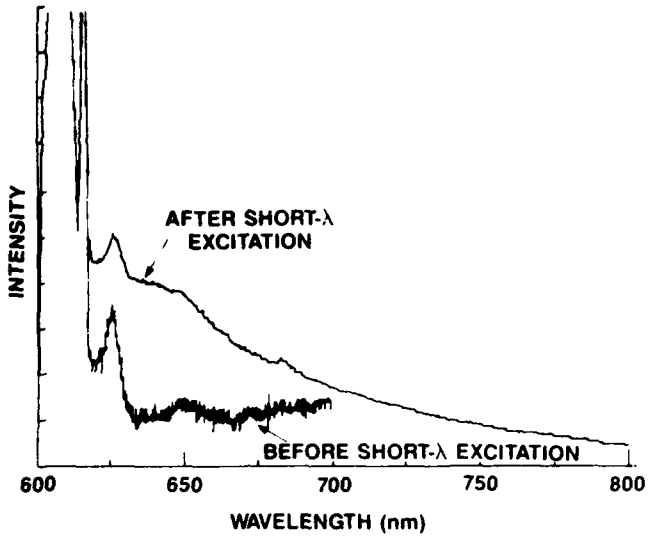

Figure 9. Comparison of luminescence intensity before and after 482-nm excitation for pristine fiber. The excitation wavelength was 568 nm. The sharp structure at left is Raman scattering which was used to scale the intensitites.

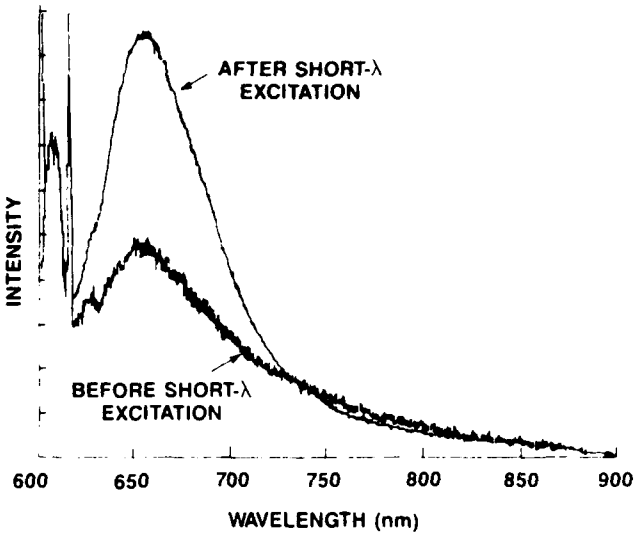

Figure 10. Comparison of luminescence intensity before and after the 482-nm excitation for fiber which was treated with hydrogen prior to irradiation. The excitation wavelength was 568 nm. The sharp structure at left is Raman scattering which was used to scale the intensities

Summary

In conclusion, we observed an improvement in radiation hardness for hydrogen-treated Ge/P- and Ge/F-codoped fibers. Treatment with hydrogen converts certain types of defects into defects which do not form deleterious color centers when irradiated. This defect conversion interpretation is supported by the photoluminescence measurements.

Acknowledgments

The authors thank R.M. Klein for encouragement as well as helpful discussions, and D. Briere, B.A. Thompson, R. Morrison, R. Scalisi, D. Carr, D. Rhodes, P. Maxwell, and J. Reese for technical assistance. This work was sponsored in part by the Rome Air Development Center at Hanscom Air Force Base, Massachusetts.

References

1. Acocella, J.; Takata, M.; Tomozawa, M.; and Watson, E.B., *J. Am. Ceram. Soc.*, Vol. 64, p. C-83. 1981. Acocella, J.; Takata, M.; Tomozawa, M.; Watson, E.B.; and Warden, J.T., *J. Am. Ceram. Soc.*, Vol. 65, p. 407. 1982.

2. Friebele, E.J.; Sigel, G.H., Jr.; and Gingerich, M.E., in *Fiber Optics: Advances in Research and Development*, p. 335, B. Bendow and S.S. Mitra, Eds., Plenum Press 1979.

3. Rush, J.D.; Beales, K.J.; Cooper, D.M.; Duncan, W.J.; and Rabone, N.H., *Br. Telecom. Technol. J.*, Vol. 2, p. 84. 1984.

4. Friebele, E.J.; Schultz, P.C.; and Gingerich, M.E., *Appl. Opt.*, Vol. 19, p. 2910. 1980.

5. Marrone, M.J., *Appl. Phys. Lett.*, Vol. 38, p. 115. 1981. Carvalho, W.; Dumas, P.; Corset, J.; and Neumann, V., in *Proceedings of Optical Fibers in Adverse Environments*, SPIE Vol. 404, p. 76. 1983. Friebele, E.J.; Griscom, D.L.; and Marrone, M.J., *J. Non-Cryst. Solids*, Vol. 71, p. 133. 1985.

APPENDIX B

Reprinted from Mat. Res. Soc. Symp. Proc. Vol. 88 – Optical Fiber Materials and Processing

Effects of Defect Modification and Reduction Techniques on the Radiation Sensitivity of Optical Fibers

T. Wei, M.P. Singh, and W.J. Miniscalco

GTE Laboratories Incorporated
40 Sylvan Road
Waltham, MA 02254

J.A. Wall

Rome Air Development Center:ESR
Hanscom AFB, MA 01731

EFFECTS OF DEFECT MODIFICATION AND REDUCTION TECHNIQUES ON THE RADIATION SENSITIVITY OF OPTICAL FIBERS

T. WEI,* M. P. SINGH,* W. J. MINISCALCO,* AND J. A. WALL**
*GTE Laboratories Incorporated, 40 Sylvan Road, Waltham, MA 02254
**Rome Air Development Center/ESRE, Hanscom AFB, MA 01731

ABSTRACT

We have investigated the relationship of precursor defects in as-drawn optical fiber to glass composition and processing conditions in order to understand the radiation sensitivity of doped-core optical fiber. Techniques are reported for improving the radiation hardness of graded-index multimode fibers through reducing the concentration of doping- and processing-induced defects as well as modifying the residual defects in as-drawn fiber. Significant decreases in radiation-induced loss have been observed for fibers pretreated with hydrogen. An investigation of the role of drawing-induced defects indicates that a lower draw temperature produces slightly harder fiber. A study of core/clad interfacial stress revealed that such stress does not play a major role in radiation sensitivity.

Measurement techniques included in situ loss measurements at 850 nm and spectral loss measurements before and after γ irradiation. In addition, photoluminescence proved to be an effective tool for characterizing specific defect centers. It was found for Ge/P-codoped fibers that the luminescence band at 650 nm attributed to drawing/radiation induced centers has an inverse correlation with induced loss. Previously unreported emission bands have been observed, including one at 720 nm which may be related to fluorine doping.

INTRODUCTION

The objectives of this investigation are to determine what influences the radiation sensitivity of doped-core optical fiber and test these conclusions by fabricating fiber with improved radiation resistance. For γ irradiation at the dose levels under consideration [$\lesssim$ 25 krad (Si)], induced absorption is due to color centers which form when pre-existing defects in the glass trap the electrons and holes generated by ionizing radiation [1]. This suggests approaches to improving radiation resistance based upon the principles of reducing the concentration of doping- and processing-induced defects as well as passivating residual defects in as-drawn fibers. In the former category are variations in dopants, doping levels, draw parameters, and composition profile (core/clad interfacial stress). In the latter category falls postfabrication modification of deleterious defects in the fiber by techniques such as hydrogen treatment.

Graded-index multimode fibers with nominal core diameter of 50 μm and NA of 0.2 were drawn from preforms fabricated by the MCVD process. The fibers were irradiated under steady-state conditions at a dose rate of $\simeq$300 rad/min using the ^{60}Co source at RADC. The primary experimental tool was the measurement of radiation-induced loss in the fibers, including in situ monitoring at 850 nm and postirradiation spectral measurement. Differential mode attenuation (DMA) was applied to examine the effect of core/clad interfacial stresses. More selective techniques such as Raman scattering and photoluminescence were also used, and the latter demonstrated particular promise for characterizing defect centers in optical fibers. All measurements and irradiations were performed at room temperature.

DEFECT REDUCTION

Reducing the concentration of precursor defects in the as-drawn fiber decreases the amount of color center absorption induced by irradiation. It is well known that the types

concentrations of dopants strongly influence the radiation sensitivity of glass due to associated defects or changes in electron/hole affinities. In particular, phosphorus doping leads to high steady-state losses [2] while fluorine doping is much less deleterious. Gozen et al., have reported higher losses for Ge/F-codoped fiber than Ge-doped fiber [3], while Shibata and Nakahara claim codoping with fluorine improves radiation resistance [4]. We found Ge-doped and Ge/F-codoped fibers to be comparable in hardness. Other potential sources of defects include preform processing and fiber drawing. Fluorine-doped fiber was used to investigate the role of two sources of fabrication-induced defects: drawing stress [5] and core/clad interfacial stress. By varying furnace temperature and draw speed, the effect of draw parameters on radiation-induced absorption was evaluated. We also fabricated two preforms with different core/clad interfacial stresses to assess the impact of thermomechanical stress on radiation hardness.

Drawing-Induced Defects

To investigate the influence of drawing conditions, four fibers were drawn from a Ge/F-codoped preform at two different values each of temperature and speed designed to vary the induced defect concentration among these fibers. The two temperatures differed by 55°C. Table I summarizes the draw parameters and radiation-induced loss data on these fibers.

Table I. Summary of results for the investigation of drawing parameters

Fiber Designation	Temp. Temp.	Draw Parameters Speed (m/s)	Tension (g)	Radiation-Induced Loss at 1000 nm	at 1300 nm
A	low	0.5	25	0.39	0.10
B	low	1.0	50	0.41	0.01
C	high	0.5	14	0.55	0.17
D	high	1.0	25	0.56	0.21

Overall, the fibers drawn at the lower temperature and speed showed slightly lower radiation-induced loss at wavelengths $\geq$1000 nm. It is generally believed that fiber drawn at a lower temperature has a lower fictive temperature and, consequently, a lower defect concentration. This is in agreement with our experimental results. The influence of draw speed is less clear and further study over a broader range will be needed to clarify it.

Stress-Induced Defects

Thermomechanical stresses arise in optical fiber because of the different thermal characteristics of core and cladding glasses. To examine the effect of core clad interfacial stress, we prepared two matched-clad preforms with the same Ge/F core composition but different cladding compositions. The first one had a pure silica cladding and provided a high core/clad stress. The second minimized the core/clad stress through the use of a Ge/F-codoped cladding matched to the refractive index of pure silica. Electron microprobe results confirmed that high concentration gradients for both Ge and F exist across the core/clad interface in the first preform, in contrast to slowly varying profiles for the second preform. The preforms were drawn into fibers using two draw speeds. Fibers designated HA and HB were drawn from the preform with a high core/clad stress, while fibers designated LA and LB were drawn from the low stress preform. Table II summarizes results on radiation-induced loss for these four fibers and reveals a slight reduction in loss at 850 nm for fibers with a low core/clad stress.

To further clarify the stress effect, the DMA technique was applied to monitor the induced attenuation of specific groups of modes. Figures 1 and 2 show DMA results at 1300 nm for fibers of high and low stress, respectively. In general, the DMA value is higher for the higher modes. Before irradiation the stress causes a steady increase in attenuation

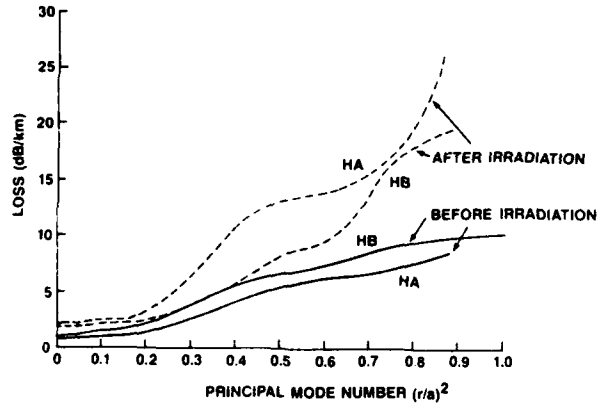

Fig. 1. Comparison of DMA results before and after 20 krad irradiation for fibers drawn from high stress preform.

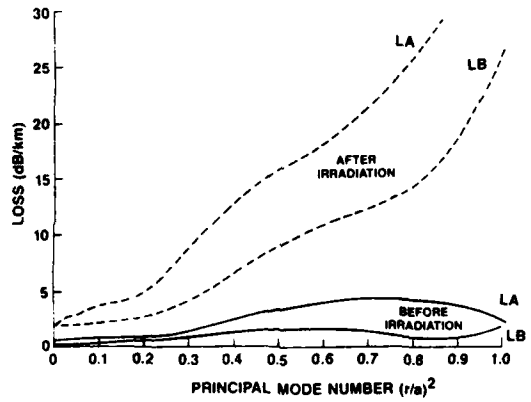

Fig. 2. Comparison of DMA results before and after 20 krad irradiation for fibers drawn from low stress preform.

with increasing mode number. For a low stress fiber the increase is slight and gradual. After irradiation, we do not observe any significant difference in DMA between fibers with different stresses. Since the spectral loss measurements used mode filters to eliminate the higher modes, the DMA data do not correlate well with the loss measurement.

Table II. Summary of Results for the Investigation of Stress Reduction

Fiber Designation	Draw Speed (m/s)	Radiation-Induced Loss at 850 nm	(dB/km/krad) at 1300 nm
HA	0.5	1.55	0.03
HB	1.0	1.55	0.14
LA	0.5	1.51	0.11
LB	1.0	1.29	0.07

The DMA results suggest that stress introduces defects only near the core clad interface, resulting in higher attenuation for higher modes. Since the higher modes do not propagate a great distance in a fiber, stress reduction may not contribute significantly to radiation hardness. Moreover, the absence of significant differences in the radiation-induced attenuation of the higher modes implies that the stress-related defects are either not great in number of not sensitive to γ radiation.

HYDROGEN TREATMENT

An approach to preventing the residual defects in as-drawn fiber from forming deleterious color centers is to convert them into benign defects prior to irradiation. The latter are defects which do not form centers with significant absorption in the spectral region of interest when irradiated. Since hydrogen is known to react with defects in fibers [6], the effects of hydrogen treatment on defect modification and the consequent radiation hardness of optical fibers have been examined [7]. This was done by comparing the radiation hardness of a treated fiber with that of an untreated fiber drawn from the same preform. Both Ge/P- and Ge/F-codoped fibers were investigated, and an improvement in radiation resistance was observed for both types. Photoluminescence was used to obtain additional insight into the distribution of defects as a function of fiber history.

Ge/P-codoped Fibers

A section of Ge/P-codoped fiber was treated in an atmosphere with a hydrogen partial pressure of 0.86 atm at 65 °C for 7 days. Both treated and untreated fibers were then irradiated to a total dose of $\simeq 5$ krad. Figure 3 compares the loss spectra after irradiation for fibers with and without the hydrogen treatment. For hydrogen-treated fiber, an improvement of $\simeq 50$ dB/km is observed in the induced attenuation at long wavelengths ($\lambda > 1\ \mu$m).

To identify specific color centers and precursor defects, sections of fiber 0.5-3m in length from the above study were subjected to photoluminescence investigation. They included an as-drawn fiber, a fiber irradiated without pretreatment, and a fiber which was hydrogen treated and then irradiated. Photoluminescence was found to be a sensitive probe of the color center population, and significant differences were detected among these fibers.

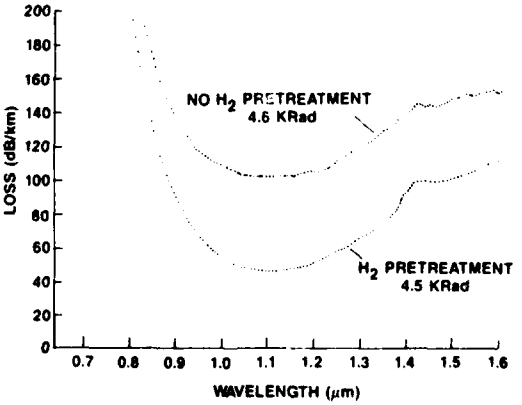

Fig. 3. Loss spectra after irradiation for fibers with and without hydrogen pretreatment (0.86 atm, 65 °C, 7 days).

Figure 4 compares the luminescence intensity excited at $\lambda_{ex} = 568$ nm for these three fibers prior to short wavelength ($\lambda < 530$ nm) photobleaching. The comparison of intensities was rendered absolute by normalizing the luminescence intensity to the 1060 cm^{-1} Raman line of silica. The 650 nm emission and a corresponding absorption band at 630 nm are induced by both the drawing process and irradiation. They have been variously attributed to the nonbridging oxygen hole center (NBOHC) [8] or a composite of the NBOHC and a nonparamagnetic electron trap [9]. This center has no significant emission for the as-drawn fiber but is prominent for the irradiated fibers, being even more intense for the fiber which had been hydrogen treated before irradiation. For the irradiated fibers, Figure 4 reveals an inverse relationship between radiation-induced loss at wavelengths >1 μm (Figure 3) and the concentration of the center emitting at 650 nm, implying that this center is not primarily responsible for the induced long-wavelength loss in these fibers. Moreover, it appears that hydrogen treatment can convert defects which will result in long wavelength losses into less deleterious defects such as the 650 nm center. For blue excitation ($\lambda_{ex} <$ 500 nm), the 650 nm emission band is replaced by a broader, more intense band peaking at $\simeq$680 nm which has not been previously reported. This second luminescence band is clearly attributable to a second type of color center based upon the differences in excitation and emission spectra as well as photobleaching characteristics.

Additional evidence for the defect conversion process was obtained through a photobleaching investigation. Prolonged excitation at short wavelengths ($\lambda < 530$ nm) produced significant photobleaching in the irradiated fibers. This occurs through photoconversion of centers and was observed as changes in photoluminescence intensity for all fibers, including the unirradiated fiber. Figure 5 illustrates the photoconversion effect for the fiber irradiated without hydrogen pretreatment. The 650 nm band increases significantly, implying an increase in concentration of the center, although the induced loss has been reduced through photobleaching. A corresponding decrease of intensity is observed for the blue-excited 680 nm band.

The photoluminescence investigation provides further support for the observation that radiation resistance can be improved by defect modification following fiber drawing. The center responsibility for the 650 nm band is an example of a relatively benign defect which can be formed by hydrogen treatment from more deleterious defects.

Ge/F-codoped Fibers

Doping with fluorine rather than phosphorus significantly improves the steady-state

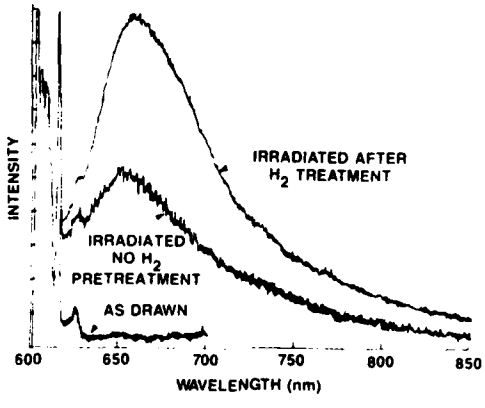

Fig. 4. Comparison of luminescence intensity prior to photobleaching for Ge P-codoped fibers, $\lambda_{ex} = 568$ nm. Sharp structure at left is Raman scattering used to normalize intensities.

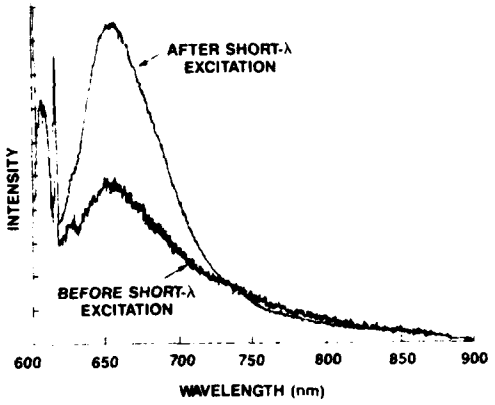

Fig. 5. Comparison of luminescence intensity before and after blue photobleaching for Ge/P-codoped fiber which was irradiated without hydrogen treatment. λ_x = 568 nm. Sharp structure at left is Raman scattering used to normalize intensities.

radiation resistance of fiber. To determine if still further improvement can be obtained through hydrogen treatment, Ge/F-codoped fibers from the core clad interfacial stress experiments were selected for investigation. Two sections of fibers HA and LA were treated in 4 atm hydrogen at 50°C for 10 days and then irradiated to a total dose of $\simeq$18 krad. Figure 6 compares loss spectra before and after irradiation for the hydrogen-treated fiber LA. Similar data were observed for fiber HA. Table III summarizes the induced loss results for fibers with and without hydrogen treatment. The treated fibers show $\simeq$15% improvement in radiation resistance at 850 nm over untreated fibers. While not as dramatic as the improvement observed for Ge/P-codoped fiber, these measurements demonstrate the effectiveness of hydrogen treatment in enhancing radiation hardness even for fiber with low radiation sensitivity. Fluorine doping leads to a lower concentration of deleterious defects than phosphorus doping and results in reduced sensitivity to radiation. Nevertheless, sufficient numbers of defects remain to provide reaction sites for hydrogen, hence the improved resistance of the treated fibers.

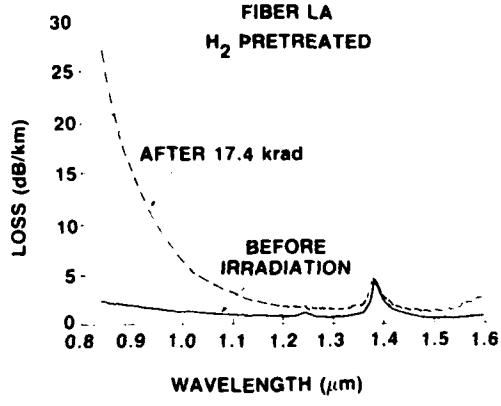

Fig. 6. Loss spectra of hydrogen-pretreated low stress fiber LA before and after irradiation.

Table III. Summary of Results for the Investigation of Hydrogen Treatment

Fiber Designation	Hydrogen Treatment	Radiation-Induced Loss at 850 nm	(dB/km/krad) at 1300 nm
HA	no	1.55	0.03
HA	yes	1.28	0.08
LA	no	1.51	0.11
LA	yes	1.29	0.04

Photoluminescence spectra were measured for irradiated and unirradiated samples of fiber LA with and without the hydrogen treatment. Figure 7 compares luminescence intensity at λ_{ex} = 568 nm for these fibers before photobleaching. A broad emission band peaking at $\simeq$720 nm is observed for all Ge/F fibers, which is in contrast to the dominant band at 650 nm for Ge/P fibers (Figure 4). Even for irradiated Ge/F fibers, only a shoulder at 650 nm is observed. When the excitation wavelength is shortened, the 720 nm band increases in intensity and shifts to shorter wavelength. Under blue excitation (λ_{ex} = 476-488 nm), this band peaks at $\simeq$680 nm and is identical to that observed for the Ge/P fibers. This suggests that a single type of center with an extremely inhomogeneous distribution of sites is responsible for this emission for both types of fiber. As with the Ge/P fibers, the 680/720 nm band in Ge/F fibers is significantly bleached by blue excitation. Only subsequent to photobleaching is the 650 nm band clearly observed for λ_{ex} = 568 nm. This effect is illustrated in Figure 8 for fiber LA which was irradiated without hydrogen treatment.

The results for the Ge/F fibers add to the evidence that two distinct defect centers absorbing in the visible are responsible for the 650 nm and 680/720 nm emission bands. The center emitting at 680/720 nm is present at a greater concentration in the Ge/F fibers than in the Ge/P fibers. Conversely, there seems to be a greater number of the 650 nm defects in the Ge/P fibers. We tentatively attribute the 720 nm emission band observed only for Ge/F fibers to fluorine-perturbed sites of the 680 nm center which emit and absorb at longer wavelengths than the majority of the defect sites.

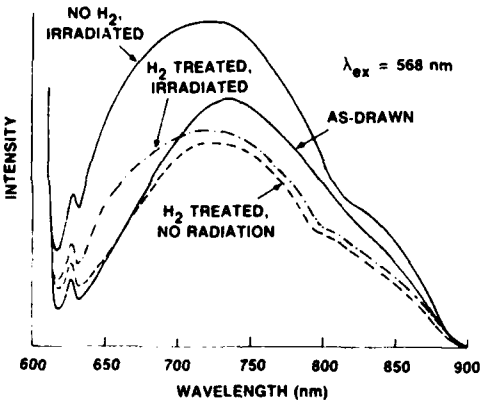

Fig. 7. Comparison of luminescence intensity prior to photobleaching for Ge/F-codoped fibers.

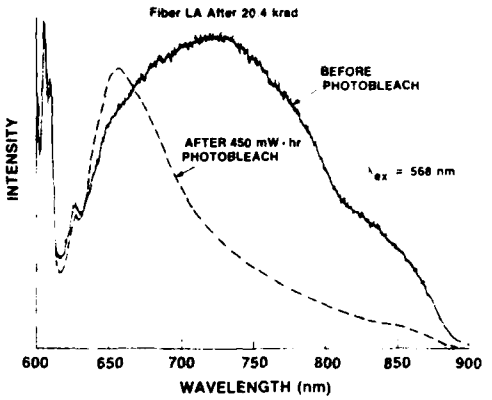

Fig. 8. Comparison of luminescence intensity for Ge/F-codoped fiber before and after photobleaching at 488 nm. Fiber had been irradiated to 20.4 krad without hydrogen pretreatment. Sharp structure as left is Raman scattering used to normalize intensities.

CONCLUSION

It is generally recognized that radiation-induced loss in optical fiber is a sensitive function of the specific dopants used for fining and index control. Our investigations indicate that the types of dopants have a more significant effect upon the defect concentration in as-drawn fiber than the processing conditions. Fluorine doping leads to harder fiber than phosphorus doping, and photoluminescence reveals that it appears to modify certain defects. This is consistent with a recent molecular dynamics simulation of a Ge/F-codoped glass which found a large Ge-F affinity [10]. Techniques for reducing the number of fabrication-induced defects have a relatively minor effect upon radiation hardness. However, passivation through hydrogen treatment of precursor defects in as-drawn fiber in an effective means of reducing radiation sensitivity even for fiber with low defect concentrations.

ACKNOWLEDGEMENT

The authors thank R. M. Klein for many helpful suggestions and are indebted to D. Briere, D. Carr, P. Maxwell, J. Reese, D. Rhodes, R. Scalisi, and B. A. Thompson for technical assistance. This work was sponsored in part by the Rome Air Development Center at Hanscom Air Force Base, Massachusetts.

REFERENCES

1. For a review see E. J. Friebele, K. J. Long, C. G. Askings, M. E. Gingerich, M. J. Marrone, and D. L. Griscom, SPIE 541, 70 (1985)
2. E. J. Friebele, P. C. Schultz, and M. E. Gingerich, Appl. Opt. 19, 2910 (1980)
3. T. Gozen, H. Tanaka, A. Utsumi, T. Maeda, and S. Okamoto, Proc. 1984 Conf. on Elect. Insul. and Dielect. Phenomena, (IEEE, Piscataway, NJ, 1984), p. 65
4. S. Shibata and M. Nakahara, J. Lightwave Technol. LT-3, 860 (1985)

5. H. Hanafusa, Y. Hibino, and F. Yamamoto, Elect. Lett 22, 106 (1986).
6. A. Tomita and P. J. Lemaire, Elect. Lett. 21, 71 (1985).
7. T. Wei, M. P. Singh, W. J. Miniscalco, and J. A. Wall, SPIE 721, in press.
8. L. N. Skuja, A. R. Silin, and A. G. Boganov, J. Non-Cryst. Solids 63, 431 (1984).
9. E. J. Friebele, D. L. Griscom, and M. J. Marrone, J. Non-Cryst. Solids 71, 133 (1985).
10. P. I. K. Onorato (*private communications*).

APPENDIX C

Reprinted from SPIE Vol. 842 –

Fiber Optics Reliability: Benign and Adverse Environments

Effect of Fluorine Doping on Radiation Hardness of Graded Index Optical Fibers

T. Wei, M.P. Singh, and W.J. Miniscalco

GTE Laboratories Incorportated
40 Sylvan Road
Waltham, MA 02254

P.I.K. Onorato

PIKO Associates
2 Lee Anne Circle
Sudbury, MA 01776

J.A. Wall

Rome Air Development Center:ESR
Hanscom AFB, MA 01731

Effect of fluorine doping on radiation hardness of graded index optical fibers

T. Wei, M.P. Singh, and W.J. Miniscalco
GTE Laboratories Incorporated
40 Sylvan Road, Waltham, Massachusetts 02254

P.I.K. Onorato
PIKO Associates
2 Lee Anne Circle, Sudbury, Massachusetts 01776

and

J.A. Wall
Rome Air Development Center/ESRE
Hanscom AFB, Massachusetts 01731

ABSTRACT

We report an experimental and theoretical investigation of the effects of doping and processing on precursor defects in graded index multimode fibers. Fabrication parameters that significantly influence radiation sensitivity have been identified. In particular, we examined the role of fluorine doping in defect formation and its relationship to radiation sensitivity.

The experimental effort included fiber fabrication and radiation-induced loss measurements on graded index, Ge-doped core fibers. Fluorine was added to the core and/or the cladding of test fibers. Two critical parameters, barrier layer thickness and core dopants, have been identified and correlate with induced loss. In addition, the reproducibility of both fiber fabrication and measurement with respect to induced loss has been tested and found to be excellent. Induced loss was found to be proportional to Ge concentration in the core; however, the trend with fluorine doping was less clear.

The experimental results are consistent with molecular dynamics simulations which indicate the types and numbers of structural defects in the glasses. The simulations revealed significant differences in defect types and concentrations among glass compositions that included pure silica, Ge-doped silica, and Ge/F-codoped silica. Fluorine codoping decreases the number of germanium-related defects but increases the number of defects associated with silicon.

1. INTRODUCTION

At moderate dose levels, radiation-induced loss in glass occurs when existing defects form color centers by trapping electrons and holes generated by ionizing radiation.[1] Reducing the concentration of defects in the as-drawn fiber should reduce the amount of color center absorption following irradiation. Accordingly, identifying and controlling the major sources of defects is a promising approach to more radiation-resistant fiber.[2] The underlying principle is to alter the fiber composition, design, or fabrication process in order to minimize the number of precursor defects in the as-drawn fiber. The most important step is then the identification of which of the above parameters significantly influence radiation sensitivity. Two critical parameters, barrier layer thickness and core dopants, have been identified and correlated with induced loss. In support of these findings, the reproducibility of both fiber fabrication and measurement with respect to induced loss has been tested.

The experimental investigations are being supplemented with molecular dynamics (MD) simulations of the glass to determine the types of defects and their concentrations. This involves computer generation of glass structures which are then analyzed to identify defects. The objective of the MD simulations is to establish the correlation between structural defects and the dopants used either to modify the index of refraction or to reduce the defect concentrations.

2. PROCEDURE

Graded-index multimode fibers with nominal core diameters of 50 μm and numerical apertures of 0.2 were drawn from preforms fabricated by the MCVD process. Both Ge-doped and Ge/Fe-codoped fibers have been prepared. The fibers were irradiated under steady-state conditions at a dose rate of 300 rad/min using the ^{60}Co source at RADC. The primary experimental tools were preirradiation and postirradiation spectral measurements. More selective techniques such as Raman scattering, photoluminescence, and photobleaching were also used to characterize specific defects in optical fibers. The optical investigations have been reported previously[2] and will not be discussed here.

Molecular dynamics simulations were done by calculating the pairwise interionic forces of a large array of ions. The net force on each ion was then used to determine its velocity and position slightly later in time. The new positions were used in turn to

recalculate the interionic forces. This process was iterated until an equilibrated structure was reached. The equilibration temperature was 6000 K, which provided the ions with considerable mobility and resulted in thorough mixing in a very short period of time. After equilibration, the glass was cooled to room temperature by removing kinetic energy in several steps, i.e., slowing the ions.

The program used to generate the glasses required empirical parameters that characterize the interionic forces for each of the species. These parameters were chosen by adjusting their values until the average interionic distances agreed with experimental values. The array was limited to 180 ions to make the computational problem tractable. Because of the small sample size, accurate statistics were obtained using multiple configurations of the same basic cell. The location of each ion in each configuration was saved and separate computer programs were used to analyze the structure.

3. INVESTIGATIONS OF PROCESS- AND DOPING-RELATED DEFECTS

3.1. Reproducibility of fiber drawing and loss measurements

A major issue in any study of radiation effects is that of the reproducibility of the results. In the present investigation, the consistency of the fiber drawing conditions, irradiation, and loss measurements with respect to radiation-induced loss was explicitly examined. This was done by drawing new fibers from existing preforms from which fiber had been drawn and tested approximately one year earlier. The new fibers were then γ-irradiated at RADC to a nominal dose of 20 krad, and the induced losses were compared at 850, 1000, and 1300 nm (Table 1). In the fiber designation column, the number 1 or 2 indicates the first or second fiber drawing, respectively. The induced losses for two fibers drawn from the same preform are nearly identical except at 1300 nm, where the values are too low for accurate measurements.

Previous experiments had established that, within the range investigated, drawing conditions have a relatively minor effect upon radiation hardness.[2] Taken together, these results indicate that preform composition (including intentional dopants and unintensional impurities) is more important than processing conditions in determing radiation sensitivity. Indeed, the induced loss at a given wavelength is virtually the same for all the Ge/F-codoped fibers (HA, LA, and HD). If the results for the three fibers are averaged, one obtains 1.49 ± 0.04 dB/km/krad at 850 nm, 0.33 ± 0.04 dB/km/krad at 1000 nm, and 0.06 ± 0.04 dB/km/krad at 1300 nm. Fibers LD have lower sensitivities at the shorter wavelengths but are identical to the Ge/F-codoped fibers at 1300 nm. These fibers contain no fluorine in the core and have a low germanium concentration.

Table 1. Reproducibility of Radiation-Induced Loss Measurements

Fiber Designation	Radiation-Induced Loss (dB/km/krad) 850 nm	1000 nm	1300 nm
HA-1	1.55	0.30	0.03
HA-2	1.43	0.34	0.12
LA-1	1.51	0.39	0.11
LA-2	1.49	0.29	0.03
HD-1	1.50	0.34	0.05
HD-2	1.48	0.29	0.01
LD-1	1.03	0.24	0.07
LD-2	1.01	0.23	0.06

3.2. Effect of barrier layer thickness on radiation-induced loss

In the course of investigating the effects of fabrication parameters, we discovered that the radiation hardness correlates well with the barrier layer thickness. Figure 1 compares the induced loss for fibers with 10 and 20 barrier passes deposited on the inside of the fused quartz substrate tube conventionally used in the MCVD process. It is proposed that defect centers responsible for the induced loss are associated with impurities, e.g., alkali ions, that diffuse into the core from the low-purity substrate tube. The impurities must diffuse through the high-purity barrier layer whose thickness is roughly proportional to the number of barrier deposition passes. There is evidence in the literature that suggests that alkali and aluminum ions can diffuse into the fiber core from the substrate tube during the fabrication process.[3,4] Impurities introduced in this way have been shown to increase the radiation sensitivity of Ge-doped fibers.[3] Alkali ions are known to enter the network interstices and generate nonbridging oxygens for charge compensation. Although Figure 1 indicates that a significant reduction in induced loss can be obtained by increasing the barrier thickness, the practical limit for such improvement remains to be determined.

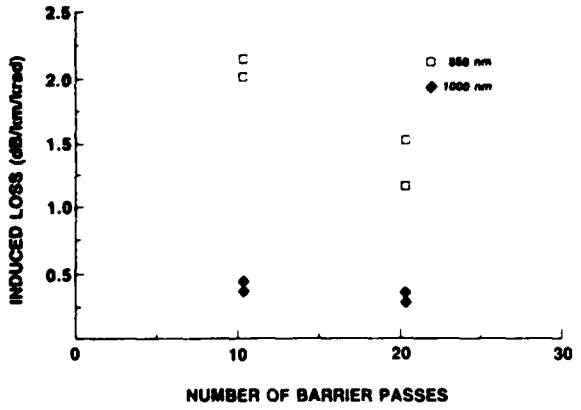

Figure 1. Radiation-induced loss as a function of the number of barrier passes on a fused quartz substrate tube. Losses were measured at 850 and 1000 nm.

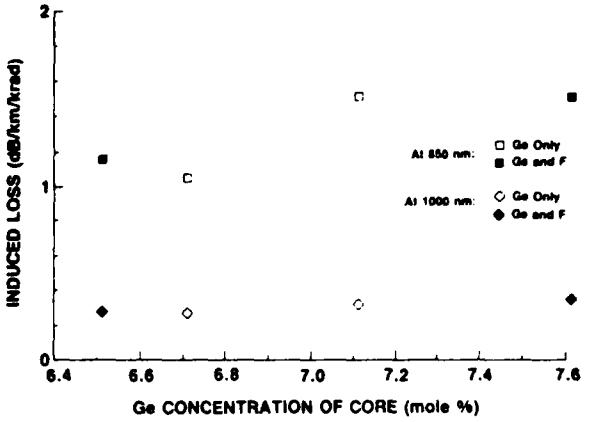

Figure 2. Radiation-induced loss as a function of the Ge concentration of the fiber core. Losses were measured at 850 and 1000 nm. Empty symbols are fibers doped only with Ge in the core; filled symbols are fibers codoped with both Ge and F in the core.

3.3 Effect of fluorine doping

The preceding discussion of the role played by impurities has a direct bearing on intentional dopants since the latter are expected to produce similar effects. Since an index modifying dopant is essential to graded index fiber, we have addressed the question of how dopant types and concentrations affect radiation sensitivity. Germanium and fluorine are the dopants included in this ongoing investigation. We are particularly interested in studying fluorine as a core dopant because of the controversy surrounding its effects. Gozen et al. have observed higher losses for Ge/F-codoped fiber than for Ge-doped fiber,[5] while Shibata and Nakahara have reported that codoping with fluorine improves radiation resistance.[6]

As part of this investigation, we fabricated four preforms with different Ge and F concentrations in the core, including two without fluorine. Table 2 lists the core and clad dopant concentrations as well as the radiation-induced loss data for these fibers. The results are also illustrated in Figure 2, which indicates the expected trend of increasing induced loss with increasing Ge concentration in the core. However, the trend with F doping is less clear and it is not known if the variations shown are significant or fall within the range of experimental uncertainty. Additional experiments are in progress to clarify the role of fluorine doping in radiation sensitivity.

Table 2. Effects of Dopant Types and Concentrations on Radiation-Induced Loss

Fiber Designation	Core Ge (mole %)	Core F (mole %)	Clad F (mole %)	Radiation-Induced Loss (dB/km/krad) 850 nm	1000 nm	1300 nm
HD	7.6	2.1	2.1	1.49	0.32	0.03
MD	6.5	0.9	2.1	1.13	0.25	0.04
LD	6.7	0	0	1.02	0.24	0.07
861117	7.1	0	0	1.49	0.29	0.06

4. MOLECULAR DYNAMICS SIMULATIONS

Five glass compositions have been generated by molecular dynamics, and three of these will be discussed. They are pure SiO_2, SiO_2 doped with 10 mole % GeO_2 (G6S54), and SiO_2 doped with 10 mole % GeO_2 and 5 anion % fluorine (F6G6). The analysis programs calculated the radial distribution function (RDF) of each type of ion pair, the probability of various types of bonds and nearest neighbors, and the distribution of intratetrahedral and intertetrahedral bond angles. On the basis of the RDFs, definitions of normal (–), stretched (· ·), and nonexistent bonds were made.

4.1. Radial distribution functions

The Si–O RDFs for the three glasses are shown in Figure 3. The average Si–O bond length is longer in the doped glasses than in pure silica. The unrestricted Si–O RDFs (i.e., for all Si ions) for the Ge-doped and the Ge/F-doped glasses are virtually identical, and only the latter is shown. For the doped glasses there are, however, restricted RDFs (i.e., subject to some condition) that are radically different. This is illustrated in Figure 3 for the Ge/F doped glass: the Si–O RDF calculated subject to the condition that the Si ions have a normal bond to a fluorine is compared to that for Si ions with a stretched bond to a fluorine. The most probable Si–O bond length for Si ions that also form normal Si–F bonds is the same as that of pure SiO_2. However, these Si ions form fewer longer than average Si–O bonds than those found in pure SiO_2, indicating that SiO_3F tetrahedra are tightly bound. This is not surprising since this complex has excess positive charge and less repulsion among the anions. The Si–O RDF for Si ions that form stretched Si–F bonds shows a wide distribution of bond lengths, indicating a variety of Si coordinations.

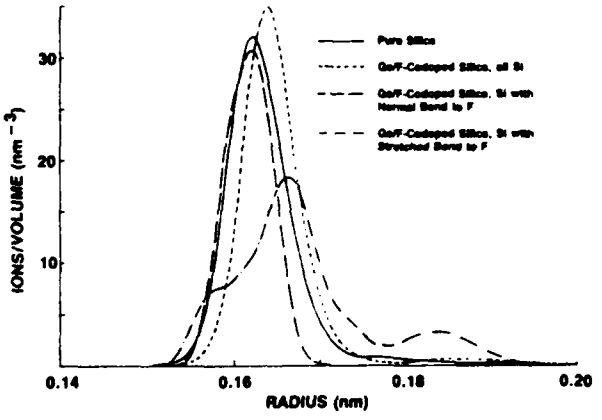

Figure 3. Si–O radial distribution functions for pure silica and Ge/F-codoped silica. The unrestricted RDF for Ge-doped silica is indistinguishable from that of the codoped glass.

When fluorine is added to the Ge-doped glass (composition F6G6), the long-distance tail of the Ge–O RDF disappears, even though the Ge–O bond distance for Ge ions also bonded to F is greater than the average bond length for all Ge ions in any of the Ge-containing glasses (Figure 4). The Ge–F RDF itself is quite interesting (Figure 5), showing two distinct classes of Ge–F bonds. By examining the nearest neighbors for Ge ions in each class of Ge–F bonds, it was found that the fluorine ions that form a normal bond with Ge are terminal or nonbridging F ions. Fluorine ions that form a stretched bond with Ge are bridging and form a Ge - - F–Si unit. Overall, 16.66% of all Ge ions are bonded to one or more F ions, and 16.18% are bonded to two F ions. This indicates a high affinity between Ge and F since only 1.16% of the Ge ions would be bonded to two fluorines if the Ge and F ions were randomly distributed throughout the network. Moreover, approximately 85% of the Ge ions are 4-coordinated and 16% of the Ge ions are 5-coordinated, with two of the neighbors being F ions.

The effect of fluorine on the Si coordination in the codoped glass is even more complicated. The analysis indicates that 93.09% of the Si ions are 4-coordinated, some including one F ion; 6.82% of the Si ions are 5-coordinated, again some including one F ion; and 0.09% of the Si ions are only 3-coordinated. The latter complexes may be precursors to E′ centers which would form if a 3-coordinated Si trapped an electron at the site of the "missing" oxygen. The 5-coordinated silicons may be the simulation's attempt to produce the peroxyl bridge, which cannot actually be generated by a calculation using ionic potentials.

4.2. Anion environments

The coordination of the anions was examined in detail for the three glass compositions. Even in pure SiO_2, a number of defects are observed, including stretched bonds, 3-coordinated oxygens, and nonbridging oxygens (NBOs). The latter are precursors to the nonbridging oxygen hole center which forms when the NBO traps a hole. The 3-coordinated and 1-coordinated oxygens may represent an ionic approximation to valence alternation pairs.

The most significant difference in defect structure among the glasses is found in the total number of 3-coordinated oxygens. In pure SiO_2, only 1.03% of the oxygens are in 3-fold coordination. In the doped glasses, with only 10 mole % GeO_2, the fraction of oxygens in 3-fold coordination is more than twice as great as in pure SiO_2 (2.22% in G6S54 and 2.28% in F6G6). Viewing the glass as corner-connected SiO_4 or GeO_4 tetrahedra, one concludes that at least two stretched Si–O bonds or at least one stretched Ge–O bond is needed to form a 3-coordinated oxygen. Garofalini has reported finding 3-coordinated oxygens in a molecular dynamics

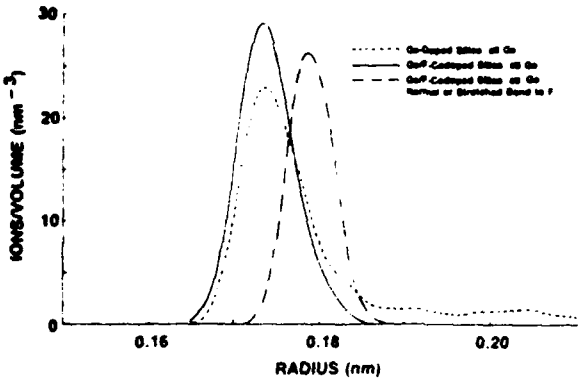

Figure 4. Comparison of Ge–O radial distribution functions for Ge-doped glasses.

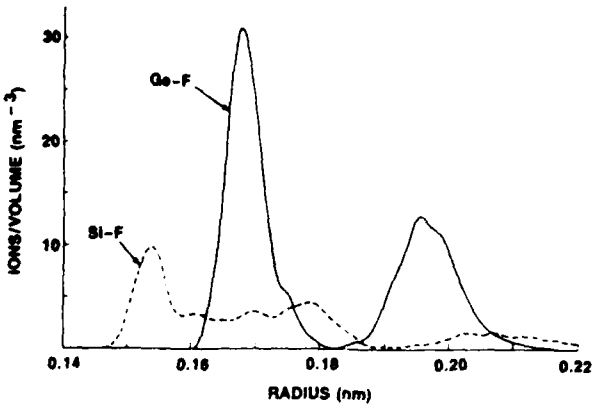

Figure 5 Si–F and Ge–F radial distribution functions for Ge/F-codoped silica.

simulation of pure silica, and he also observed that these are associated with stretched Si–O bonds.[7] A 3-coordinated oxygen can not be shared by three regular tetrahedra; they must be distorted. For the codoped glass (F6G6), the addition of fluorine eliminates 3-coordinated oxygens bonded to Ge, as well as all stretched Ge–O bonds. The latter is reflected in the Ge–O RDF in Figure 4. However, the total number of 3-coordinated oxygens does not decrease significantly because of an increase in the number of oxygens coordinated by three silicons. The effect of fluorine doping on radiation sensitivity is complex: it alters the types but not the total numbers of 3-coordinated oxygens. This ambiguity is reflected in the experimental measurements of radiation-induced loss.

5. CONCLUSION

We have investigated the effect of defect reduction on the radiation sensitivity of graded index optical fibers. Both barrier layer thickness and core dopants were found to correlate with induced loss. It was confirmed that Ge doping leads to greater sensitivity; however, both experimental and theoretical results remain ambiguous as to whether fluorine doping is beneficial or deleterious. Our study pointed out that impurities in the fiber are more important than the intrinsic defects induced by processing and fabrication in determining radiation sensitivity of optical fiber.

6. ACKNOWLEDGMENTS

The authors thank Dr. R.M. Klein for many helpful suggestions, and D. Briere, D. Carr, P. Maxwell, J. Reese, R. Scalisi, and B. Thompson for technical assistance. This work was sponsored in part by the Rome Air Development Center at Hanscom Air Force Base, Massachusetts.

7. REFERENCES

1. E.J. Friebele, K.J. Long, C.G. Askins, M.E. Gingerich, M.J. Marrone, and D.L. Griscom, "Overview of radiation effects in fiber optics," *SPIE 541*, 70-88 (1985).

2. T. Wei, M.P. Singh, W.J. Miniscalco, and J.A. Wall, "Effects of defect modification and reduction techniques on the radiation sensitivity of optical fibers," *Mater. Res. Soc. Symp. Proc. 88*, 207-215 (1987).

3. H. Hanafusa, Y. Hibino, H. Itoh, and F. Yamamoto, "Influence of impurities on loss increase in optical fiber," *Electron. Lett. 23*, 10-11 (1987).

4. M. Ogai, A. Iino, and K. Matsubara, "Behavior of alkali impurities and their adverse effect on germania doped silica fibers," Tech. Digest OFC/IOOC '87, postdeadline paper No. PDP3 (1987).

5. T. Gozen, H. Tanaka, A. Utsumi, T. Maeda, and S. Okamoto, "Radiation-resistant pure-silica core single-mode fibers," *Proc. 1984 Conf. on Electr. Insul. and Dielectr. Phenom.*, pp. 65-70 (IEEE, Piscataway, NJ 1984).

6. S. Shibata and M. Nakahara, "Fluorine and chlorine effects on radiation-induced loss for GeO_2-doped silica optical fibers," *J. Lightw. Technol. LT-3*, 860-863 (1985).

7. S.H. Garofalini, "Defect species in vitreous silica — a molecular dynamics simulation," *J. Noncryst. Sol. 63*, 337-345 (1984).

MISSION
of
Rome Air Development Center

RADC plans and executes research, development, test and selected acquisition programs in support of Command, Control, Communications and Intelligence (C^3I) activities. Technical and engineering support within areas of competence is provided to ESD Program Offices (POs) and other ESD elements to perform effective acquisition of C^3I systems. The areas of technical competence include communications, command and control, battle management, information processing, surveillance sensors, intelligence data collection and handling, solid state sciences, electromagnetics, and propagation, and electronic, maintainability, and compatibility.

Printed by
United States Air Force
Hanscom AFB, MA 01731